Available online at www.sciencedirect.com
ScienceDirect
Carbohydrate Research 342 (2007) 2097–2124
Carbohydrate RESEARCH

Conformation, dynamics, solvation and relative stabilities of selected β-hexopyranoses in water: a molecular dynamics study with the GROMOS 45A4 force field

Vincent Kräutler, Martin Müller and Philippe H. Hünenberger*

Laboratory of Physical Chemistry, ETH Zürich, CH-8093 Zürich, Switzerland

Received 24 July 2006; received in revised form 6 April 2007; accepted 1 May 2007
Available online 18 May 2007

Abstract—The present article reports long timescale (200 ns) simulations of four β-D-hexopyranoses (β-D-glucose, β-D-mannose, β-D-galactose and β-D-talose) using explicit-solvent (water) molecular dynamics and vacuum stochastic dynamics simulations together with the GROMOS 45A4 force field. Free-energy and solvation free-energy differences between the four compounds are also calculated using thermodynamic integration. Along with previous experimental findings, the present results suggest that the formation of intramolecular hydrogen-bonds in water is an 'opportunistic' consequence of the close proximity of hydrogen-bonding groups, rather than a major conformational driving force promoting this proximity. In particular, the conformational preferences of the hydroxymethyl group in aqueous environment appear to be dominated by 1,3-*syn*-diaxial repulsion, with *gauche* and solvation effects being secondary, and intramolecular hydrogen-bonding essentially negligible. The rotational dynamics of the exocyclic hydroxyl groups, which cannot be probed experimentally, is found to be rapid (10–100 ps timescale) and correlated (flip-flop hydrogen-bonds interconverting preferentially through an asynchronous disrotatory pathway). Structured solvent environments are observed between the ring and lactol oxygen atoms, as well as between the 4-OH and hydroxymethyl groups. The calculated stability differences between the four compounds are dominated by intramolecular effects, while the corresponding differences in solvation free energies are small. An inversion of the stereochemistry at either C_2 or C_4 from equatorial to axial is associated with a raise in free energy. Finally, the particularly low hydrophilicity of β-D-talose appears to be caused by the formation of a high-occurrence hydrogen-bonded bridge between the 1,3-*syn*-diaxial 2-OH and 4-OH groups. Overall, good agreement is found with available experimental and theoretical data on the structural, dynamical, solvation and energetic properties of these compounds. However, this detailed comparison also reveals some discrepancies, suggesting the need (and providing a solid basis) for further refinement.

Keywords: Glucose; Mannose; Galactose; Talose; Conformation; Dynamics; Solvation; Stability; Computer simulation; Molecular dynamics

1. Introduction

In the past few years, the scientific community has shown a renewed interest for carbohydrates,[1,2] due to the key role they play in numerous biochemical and technological processes,[3–15] as well as their potential for the design of new materials.[16] However, while experimental data on oligo- and polysaccharides (both in the solid state and in solution) are relatively abundant, the present knowledge concerning their monosaccharide building blocks remains surprisingly fragmentary (and widely scattered across the scientific literature). This is mainly because a complete understanding of monosaccharide structure and dynamics in solution requires to deal simultaneously with three difficult problems: (i) the large number of possible isomers and conformers at equilibrium for a given monosaccharide stereochemistry (constitutional isomers, anomers, ring conformers, hydroxymethyl rotamers and hydroxyl rotamers); (ii) the complex interplay between the different driving forces (steric, stereoelectronic, electrostatic and solvation effects) affecting the corresponding populations at

* Corresponding author. Tel.: +41 44 632 5503; fax: +41 44 632 1039; e-mail: phil@igc.phys.chem.ethz.ch

0008-6215/$ - see front matter © 2007 Elsevier Ltd. All rights reserved.
doi:10.1016/j.carres.2007.05.011

equilibrium; (iii) the difficulty of extracting unambiguous information on these systems based on experimental measurements, in particular in aqueous solution (multiplicity of isomers and conformers, similitude of spectroscopic properties between the different hydroxyl groups as well as between these and water, fast chemical exchange of the hydroxyl protons).

A brief summary of the isomeric and conformational equilibria that must be considered for an accurate description of solvated monosaccharides is provided below (with a focus on aldohexopyranoses in aqueous solution), together with a few key conclusions resulting from experimental investigations.

Constitution: At least six distinct constitutional isomers may be present at equilibrium in solution, namely[17–25] the α- and β-pyranose forms (six-membered rings), the α- and β-furanose forms (five-membered rings), and the (free or hydrated) acyclic forms (free carbonyl and hydrate). Septanose forms[26–28] (seven-membered rings) are not observed for aldohexoses in water.[28–30] Constitutional changes (mutarotations) are typically associated with timescales[17,25,31–36] of the order of 10^3 s, and the relative populations of the corresponding species may be readily determined via nuclear magnetic resonance[18,19,21,22,24,37] (NMR) or complexation[38,39] studies. For aldohexoses in aqueous solution, the α- and β-pyranose forms (mixture) are the leading constitutional isomers. The contribution of the furanose forms is below 10% for all aldohexoses[24] except altrose, idose and talose (about 30%), while that of acyclic isomers is below 0.1% in all cases[21,22,24,40] except for idose (about 1%).

Ring conformation: Pyranose systems may present at least eight relevant conformers in solution[1,2,18,20,41–44] (which are most easily distinguished geometrically by means of appropriate pseudorotation variables[20,45–53]), namely two chair forms (originally labelled C1 and 1C or, more recently, $^4C_1$ and $^1C_4$) and six boat forms (labelled $^{1,4}B$, $^{2,5}B$, $^{3,0}B$, $B_{1,4}$, $B_{2,5}$ and $B_{3,0}$). Skew-boat forms may also be of relevance for some systems.[48,54–65] For a given monosaccharide stereochemistry, the relative free energies of the different pyranose ring conformations in aqueous solution may be estimated using empirical additive schemes (e.g., Hassel-Ottar,[66] Reeves-Kelly,[38,41] Angyal[18,67] and Corey-Feiner[68,69] schemes). These schemes were derived from experimental complexation[38,39,41,70,71] and NMR[18,67,72] measurements on model six-membered ring compounds. Other estimates have been provided by molecular-mechanical[49,50,73–77] or quantum-mechanical[78–81] analyses. For nearly all aldohexopyranoses of the D-series, the $^4C_1$ chair conformation appears to be the only significantly populated ring conformer in aqueous solution.[41,82] Exceptions are generally characterized by the presence (or dominance) of a $^1C_4$ conformation[18,19,21,22,30,41,49,67,83–85] (for D-altrose, D-idose and, possibly, D-gulose; more populated for the α- compared to the β-anomers). For aldohexopyranoses of the L-series, this behavior is inverted (e.g., the $^1C_4$ conformation of a β-L-hexopyranose is the mirror image of the $^4C_1$ conformation of the corresponding β-D-hexopyranose). Ultrasonic-relaxation spectroscopy[36,86–88] and NMR[89] measurements suggest that chair–chair interconversion in aldohexopyranoses takes place on the μs timescale (it may occur on the 100 ns timescale if a boat or skew-boat intermediate is thermally accessible). Another study placed the interconversion between the two chair forms of the penta-acetylated idopyranose ring on the 50 ns timescale.[61]

Conformation of the exocyclic hydroxymethyl group: The conformational properties of the exocyclic hydroxymethyl dihedral angle ω (C_4–C_5–C_6–O_6) in aldohexopyranoses may be investigated based on NMR coupling constants together with appropriate Karplus-type equations.[90–98] The reported conformer populations around ω (to our knowledge only available for glucose,[93,95,96,98–104] mannose[105] and galactose,[93,95,96,100,102,104] either free or O_1-methylated) show significant variations between different literature sources. However, all studies evidence a clear predominance of the g_+ and t rotamers (with comparable populations, g_- being nearly absent) for glucose and mannose. For galactose, one set of studies[93,100,102,104] suggests that the three rotamers are significantly populated, while the two most recent determinations[95,96] support a predominance of the t and g_- rotamers (with a higher population for t, g_+ being nearly absent). Ultrasonic-relaxation spectroscopy[36,87,106] and NMR[89,107,108] measurements suggest that the hydroxymethyl group rotation takes place on the ns timescale.

Conformation of the exocyclic hydroxyl groups: Experimentally, little is known about the orientational preferences and the torsional dynamics of the exocyclic hydroxyl groups in aqueous solution. This is mainly because (i) hydroxyl protons are difficult to detect via NMR spectroscopy[37,109–112] (chemical exchange, mutual overlap, overlap with solvent signal); (ii) hydroxyl group vibrations are difficult to characterize via infrared (IR) spectroscopy[110,113–115] (dual hydrogen-bond donor–acceptor character, mutual overlap, overlap with solvent bands). Furthermore, X-ray crystallography provides limited reference information in the solid state, because the hydroxyl protons are invisible in these experiments (weak diffraction centers, orientational averaging). However, detailed (although model-dependent) information concerning rotamer distributions and intramolecular hydrogen-bonding, as well as the associated timescales, may be obtained from atomistic simulations (see below).

For a given monosaccharide stereochemistry, the relative stabilities (and, thus, the associated equilibrium populations) of the different constitutional isomers, anomers, ring conformers, hydroxymethyl rotamers and

hydroxyl rotamers result from a delicate balance between many effects (often of comparable magnitudes). A brief summary of these effects is provided below (with a focus on aldohexopyranoses in aqueous solution), together with a few key conclusions resulting from experimental investigations.

Steric effects: Steric effects result from the (closed-shell) nonbonded repulsion between pairs of substituents in close spatial proximity, and should in principle be solvent insensitive. In the context of aldohexopyranoses, these include (i) the Hassel-Ottar effect[18,23,41,66,67,71,72,83,116] and other 1,3-*syn*-diaxial repulsions;[18,41,50,67–69,71,72,102,116–127] (ii) the Δ2 effect[23,41,128,129] and other vicinal-*gauche* repulsions.[18,23,50,67,69,71,72,128,129] Note, however, that the above effects may not be entirely steric in nature, that is, they may also involve a significant dipolar[126,130,131] (electrostatic) or hyperconjugative[124,132–135] (stereoelectronic) component. For example, recent articles have questioned the steric nature, magnitude, and even repulsiveness [133] of 1,3-*syn*-diaxial interactions involving aliphatic hydrogen atoms and axial substituents, suggesting that the general equatorial preference in substituted six-membered rings[42,136] is rather of predominantly hyperconjugative origin.[124,132,133,135,137]

Electrostatic effects: Electrostatic effects, mainly intramolecular hydrogen-bonding, are strongly sensitive to the nature and polarity of the solvent. Experimentally, intramolecular hydrogen-bonds in an aqueous environment can be detected only indirectly, for example, via NMR[37,109–112,115,124–126,138–149] or IR[110,113–115,144,149–153] spectroscopy. However, most studies to date have investigated model compounds (e.g., monosaccharide analogs) and only provided qualitative information on the existence or absence of a hydrogen-bond. Based on these studies, it appears that intramolecular hydrogen-bonds in aldohexopyranoses can be broadly classified into three groups in order of decreasing strength:[110,113,115,154] (i) six-membered hydrogen-bonded 'rings' between 1,3-*syn*-diaxial hydroxyl groups;[101,102,110,114,121,122,125,126,141,144–148,150,155,156] (ii) five-membered hydrogen-bonded 'rings' between cis-vicinal (axial–equatorial) hydroxyl groups;[121,150] and (iii) five-membered hydrogen-bonded 'rings' between trans-vicinal (diequatorial) hydroxyl groups.[121,150] Hydrogen-bonding interactions are strong in vacuum or in solvents of low polarity,[121,122,125,126,144,149,155] but probably represent rather weak conformational driving forces in aqueous environment.[84,142,146,150,157] For example, although hydrogen-bonds between 1,3-*syn*-diaxial hydroxyl groups in fixed orientations are always observed in water,[110,114,141,148,156] they are not always present when this orientation is conformer-dependent (e.g., when the 'ring' involves one rotatable *C–C* bond[101,102,144,150] or can only be formed in one chair conformation of a flexible six-membered ring system[121,122,125,126,149,155]). However, although sometimes questioned,[143] the existence of stable intramolecular hydrogen-bonds for monosaccharide analogs in aqueous solution has been unambiguously evidenced by NMR and IR techniques.[110,113–115,144,148] It is also supported by the results of numerous atomistic simulations of carbohydrate systems (see below). Finally, a number of studies have also underlined the importance of cooperativity effects in intramolecular hydrogen-bonding for this class of compounds.[110,115,130,154,156,158–164]

Stereoelectronic effects: Stereoelectronic effects result from the particular electronic properties associated with specific molecular fragments in specific geometries. These effects may also involve a dipolar component[165] and thus be somewhat solvent sensitive,[166,167] but this dependence should be limited compared to that of electrostatic effects. Stereoelectronic effects of relevance for aldohexopyranoses include (i) the *endo*-anomeric effect;[18,67,120,127,129,132,165–177] (ii) the *exo*-anomeric effect;[166,171–173,175,176,178–180] (iii) the *gauche* effect;[119,172,181–188] and (iv) other effects.[124,132,135,137,184,189–191]

Solvation effects: Solvation effects influence the conformational properties of carbohydrates in a very complex way.[192,193] In the context of aldohexopyranoses, they consist of a combination of the following phenomena: (i) dielectric screening of the intramolecular (mainly electrostatic, i.e., hydrogen-bonding) interactions (evidenced by numerous investigations in solvents of various polarities[84,101,102,121,122,125,126,142,144,146,148,149,151,152,155,189,190,194]); (ii) competition between intramolecular and solute–solvent hydrogen-bonds[155,195,196] (in hydrogen-bonding solvents); (iii) preferential solvation of sterically more accessible hydroxyl groups;[117,155,176,197] and (iv) specific interactions between solute hydroxyl groups and tightly bound solvent molecules or solvent bridges.[142,151,166,167,198–200] These observations have led to the proposal of several models for monosaccharide hydration: (i) the 'axial–equatorial' model[116,164,197,201–206] suggests that equatorial hydroxyl groups are more strongly hydrated compared to axial ones, because they are sterically more accessible and less likely to be involved in strong intramolecular hydrogen-bonds (see above); (ii) the 'nonspecific' hydration model[164,167] attempts to correlate the extent of hydration of the monosaccharide (hydrophilicity) with some measure of its polar solvent-accessible surface area; (iii) the 'specific' hydration model[117,192,193,198,207–216] attempts to correlate this hydrophilicity with the extent of disturbance imposed by the monosaccharide hydroxyl group geometry onto the pre-existing hydrogen-bond network of water. Although these models (as well as the four phenomena listed above) certainly capture important aspects of monosaccharide hydration, none of them seem to be currently able to account for the entire range of experimental observations.

Theoretical methods (including conformational analysis,[8,47,217–222] analysis of protein–carbohydrate interactions[223,224] and multiscale modelling approaches[225,226]) play an increasingly important role in glycobiology. Due to their remarkable spatial (individual atoms) and temporal (femtosecond) resolution, as well as their firm basis in the laws of (classical) microscopic physics, explicit-solvent molecular dynamics (MD) simulations represent a key component in many theoretical approaches. A number of force fields have been developed to represent interatomic interactions in such simulations, which can be broadly classified into three categories: (i) force fields with the primary goal of reproducing properties in vacuum or together with an implicit representation of the solvent, for example, HSEA,[179] MM2,[227] MM3,[228–230] MM4,[128,129,177,231] CFF (PEF[232]), QMFF,[233] CHARMM (QUANTA,[234] CHEAT[235,236]) and AMBER (AMBER*[237,238]); (ii) force fields with the primary goal of reproducing properties in solution together with an explicit representation of the solvent molecules, for example, CHARMM (HGFB,[239] PHLB,[240] CSFF,[241] Reiling[242] and PARM22-SU01[243]), AMBER (Homans,[244] Glennon,[245,246] Gregurick,[247] SPASIBA,[153] GLYCAM,[248–251] AMB99C[252,253] and Simmerling[254]), OPLS (AA[255] and AA-SEI[256,257]) and GROMOS (43A1,[258,259] Kouwijzer,[260,261] Ott,[262] Spieser,[263] Galema[214,264] and 45A4[265,266]); (iii) coarse-grained force fields with the primary goal of performing low-resolution simulations of large-scale systems or long timescale processes, for example, M3B.[267,268] For completeness, it should be mentioned that ab initio MD simulations of carbohydrates have also been performed.[98,269,270] The most commonly used force fields have been discussed in recent reviews,[217,219,271,272] and a number of more or less extensive force field comparisons (against vacuum,[233,273,274] solid state[275,276] or solution[273,277,278] data) have also been undertaken.

Previous simulation studies of mono- and disaccharides were carried out in vacuum or with implicit solvation,[153,237,238,252,262,270,279–282] in crystals,[260,275,283] or in water with explicit solvation, either in the finite-concentration[267,268,284–292] or in the dilute regimes. The latter explicit-solvent simulations in the dilute regime were mostly concerned with (i) the validation and refinement of carbohydrate force field parameters;[239,243,245–247,253–257,261–263,265,266] (ii) the investigation and rationalization of conformational properties[98,161,164,195,199,200,214–216,239,241,243,245–247,251,253–257,261–266,269,277,278,293–306] (e.g., intramolecular hydrogen-bonding,[161,164,195,216,277,299] rotameric populations of the hydroxymethyl group[98,241,251,293,294,305] and vibration frequencies[98,153,239,241,245–247]); (iii) the evaluation of relative free energies (between e.g., anomers,[237,238,245,254,295,296] epimers,[245,246] ring conformers[262,263,304] or hydroxymethyl rotamers[261]) or conformational entropies;[266] (iv) the investigation of carbohydrate solvation and diffusion.[98,161,164,195,199,200,214–216,245–247,264,269,277,278,296–298,300,301,303,306]

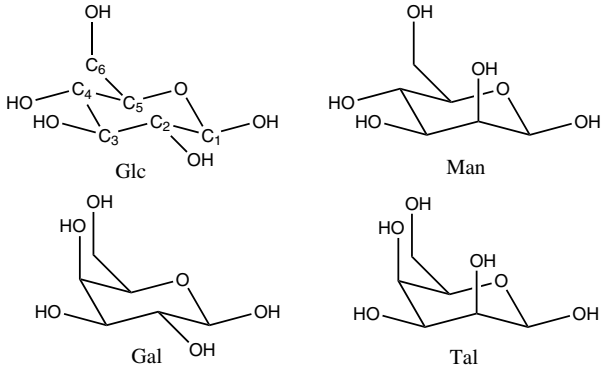

Figure 1. Chemical structures of the four β-D-aldohexopyranoses considered in the present study: β-D-glucose (Glc; including the carbon numbering scheme); β-D-mannose (Man); β-D-galactose (Gal); β-D-talose (Tal).

In the present study, a series of long timescale (200 ns) molecular simulations are performed, with the goal of providing a complete and detailed atomistic picture of the conformation, dynamics, solvation, and relative stabilities of the four aldohexopyranoses corresponding to the two possible stereochemistries at the C_2 and C_4 centers (Fig. 1): β-D-glucose (Glc), β-D-mannose (Man), β-D-galactose (Gal), and β-D-talose (Tal). This is done by comparing the results of simulations of these monosaccharides both in water and in the gas-phase. In addition, the detailed comparison of the reported results against available experimental and quantum-mechanical data also provides a critical test for the recently developed GROMOS 45A4 carbohydrate force field used in this study[265,266] (and a basis for further refinement).

Note that the literature references quoted in the present article are also listed with full titles in the Supplementary data.

2. Computational details

2.1. Molecular and stochastic dynamics simulations

All simulations were carried out using the GROMOS96[258,259] package together with the GROMOS 45A4 united-atom force field for polypeptides, nucleic acids,[307] lipids[308,309] and carbohydrates.[265,266] The four aldohexopyranoses considered were β-D-glucose (Glc), β-D-mannose (Man), β-D-galactose (Gal) and β-D-talose (Tal), see Figure 1. Throughout the article, these three-letter codes are used to refer specifically to the β-anomers. The four compounds were simulated exclusively in their pyranose ring conformation (experimentally accounting for 99.6%, 99.1%, 94.0% and 70.9%, respectively, of the corresponding total populations of constitutional isomers at equilibrium in water[24]) and in the β-anomeric

form (experimentally accounting for 62.2%, 33.2%, 66.8% and 40.5%, respectively, of the corresponding total pyranose populations[24]). The equations of motion were integrated using the leapfrog scheme with a timestep of 2 fs. All bond lengths were constrained by application of the SHAKE algorithm[310] with a relative geometric tolerance of 10^{-4}. Two sets of simulations were undertaken: (i) explicit-solvent molecular dynamics simulations[258] (MD; integrating Newton's equation of motion) in water, carried out under periodic boundary conditions; (ii) stochastic dynamics simulations[258,311] (SD; integrating Langevin's equations of motion) in vacuum.

The MD simulations employed the simple-point-charge (SPC) water model.[312] The nonbonded interactions were handled using a twin-range cutoff scheme[258] with short- and long-range cutoff radii of 0.8 and 1.4 nm, respectively, and an update frequency of 5 timesteps for the short-range pairlist and intermediate-range interactions. The mean effect of the omitted electrostatic interactions beyond the long-range cutoff distance was introduced by means of a reaction-field correction[313,314] to the short- and intermediate-range interactions based on a relative dielectric permittivity of 60, as appropriate for the SPC water model.[315,316] Solute and solvent degrees of freedom were independently coupled to a heat bath[317] at 300 K, with a relaxation time of 0.1 ps. The box dimensions were isotropically coupled to a pressure bath[317] at 1 atm, with a relaxation time of 0.5 ps and an isothermal compressibility of 45.75×10^{-5} kJ^{-1} mol nm^3. The center of mass motion was removed every 2 ps. For each of the four hexopyranoses considered, the solute was placed in a truncated-octahedron box with a minimum solute-to-wall distance of 1.6 nm, and hydrated by 970 (Glc), 963 (Man), 976 (Gal) or 976 (Tal) water molecules. To relax the system, a steepest-descent energy minimization was performed with positionally constrained ring atoms, followed by 100 ps MD equilibration prior to production.

The SD simulations in vacuum relied on a friction coefficient of 91 ps^{-1} (the value appropriate for water[258,311]) and a reference temperature of 300 K. These simulations are meant to mimic the physical situation of hexopyranoses in vacuum, but do so only approximately, because (i) the solute model parameters remain effective parameters calibrated to appropriately reproduce experimental properties in an aqueous environment[279,280,293] (enhanced partial atomic charges); (ii) the dynamical properties will be incorrect due to the application of SD (stochastic and frictional forces) rather than MD. The use of SD is selected here as a means to enhance the conformational sampling and thermostatize the system. For each of the four hexopyranoses considered, the solute was relaxed by 100 ps SD equilibration prior to production.

For both MD and SD simulations, production was carried out for a duration of 200 ns, saving trajectory frames every 0.5 ps for analysis.

2.2. Free-energy calculations

In addition to the straightforward MD (aqueous environment) and SD (vacuum) simulations (Section 2.1), free-energy calculations were performed to evaluate the relative stabilities of the four hexopyranoses in the two environments. To this purpose, a (redundant) set of six 'alchemical' epimerization processes was considered. These were carried out by inverting the signs of the improper-dihedral angles ξ controlling the stereochemistry of the centers to be inverted (C_2, C_4, or both) upon going from one hexopyranose to another one. To avoid excessive bond angle strain at the midpoint of the inversion (planar trigonal geometry at the inverting center), this change was performed in two successive steps. The first step took the center in its initial stereochemistry to an intermediate planar trigonal geometry ($\xi = 0$) with adapted reference bond angles (109.5→120°), while the second step took the trigonal intermediate to its final (inverted) stereochemistry with normal reference bond angles (120→109.5°). The corresponding changes in reference values for improper-dihedral and bond angle force field terms were performed using a linear or half-linear dependence, respectively, on a coupling parameter λ evolving from 0 (initial stereochemistry) to 1 (final stereochemistry).

The corresponding free-energy difference ΔG_{epi} was evaluated via thermodynamic integration[318–320] as

$$\Delta G_{\text{epi}} = \int_0^1 \mathrm{d}\lambda \left\langle \frac{\partial V(\mathbf{r}, \lambda')}{\partial \lambda'} \right\rangle_\lambda \qquad (1)$$

where $V(\mathbf{r},\lambda')$ is the potential energy in configuration $\mathbf{r}$ given a value λ' of the coupling parameter, and $\langle \frac{\partial V(\mathbf{r},\lambda')}{\partial \lambda'} \rangle_\lambda$ denotes ensemble (trajectory) averaging over equilibrium configurations $\mathbf{r}$ generated using a given (fixed) λ-value. In practice, the integral was replaced by a discretized version (trapezoidal rule) based on simulations at 11 equally spaced λ-points (5 ns simulation per point). Error bars were calculated using a block-average extrapolation scheme.[321]

2.3. Analysis

The analysis of the simulations was performed in terms of conformational properties (ring conformation, probability distributions of the exocyclic dihedral angles, pairwise correlations among these distributions), hydrogen-bonding (intramolecular and solute–solvent), dynamics (exocyclic dihedral transitions), solvation (spatially resolved solvent density), and relative stabilities (free-energy calculations).

The ring conformation associated with a given solute configuration along a trajectory was determined by assigning each of the six dihedral angles formed by successive ring atoms to one of three wells [0;120°],

[120; −120°], [−120; 0°]. Based on this assignment, the conformation was classified[2] as chair ($^4C_1$ or $^1C_4$), boat ($^{1,4}B$, $^{2,5}B$, $^{3,0}B$, $B_{1,4}$, $B_{2,5}$, $B_{3,0}$), or other.

To investigate the conformational properties of exocyclic dihedral angles, the following definitions were used: $\phi(O_5–C_1–O_1–H_1)$; $\chi_n(C_{n-1}–C_n–O_n–H_n$ with $n = 2,3,4,6)$; $\omega(C_4–C_5–C_6–O_6)$. Dihedral angles in the ranges [0°; 120°], [120°; −120°] and [−120°; 0°] are described as *gauche*+ (g_+), *trans* (t) and *gauche*− (g_-), respectively. These ranges appropriately encompass distinct population peaks (centered at staggered conformations) for all dihedral angles analyzed (Fig. 2). The conformation of the hydroxymethyl group is often also described in terms of the ranges to which the dihedral angles $O_5–C_5–C_6–O_6$ and $C_4–C_5–C_6–O_6$ (ω) belong, with the following correspondences: *gauche–gauche* (gg) ↔ ω in g_+; *trans–gauche* (tg) ↔ ω in g_-; *gauche–trans* (gt) ↔ ω in t.

Both intramolecular and solute–solvent hydrogen-bonds were monitored along the trajectories. A hydrogen-bond is assumed to be present when the distance between the hydrogen and acceptor atoms is below 0.25 nm, and the angle between the donor, hydrogen and acceptor atoms is above 100°. This somewhat relaxed criterion (a minimum angle of 135° is typically used instead[258]) was necessary to encompass hydrogen-bonds between vicinal hydroxyl groups (forming five-membered 'rings'). This change in the minimum angle criterion had no appreciable effect on the occurrence of nonvicinal hydrogen-bonds (forming six- or higher-

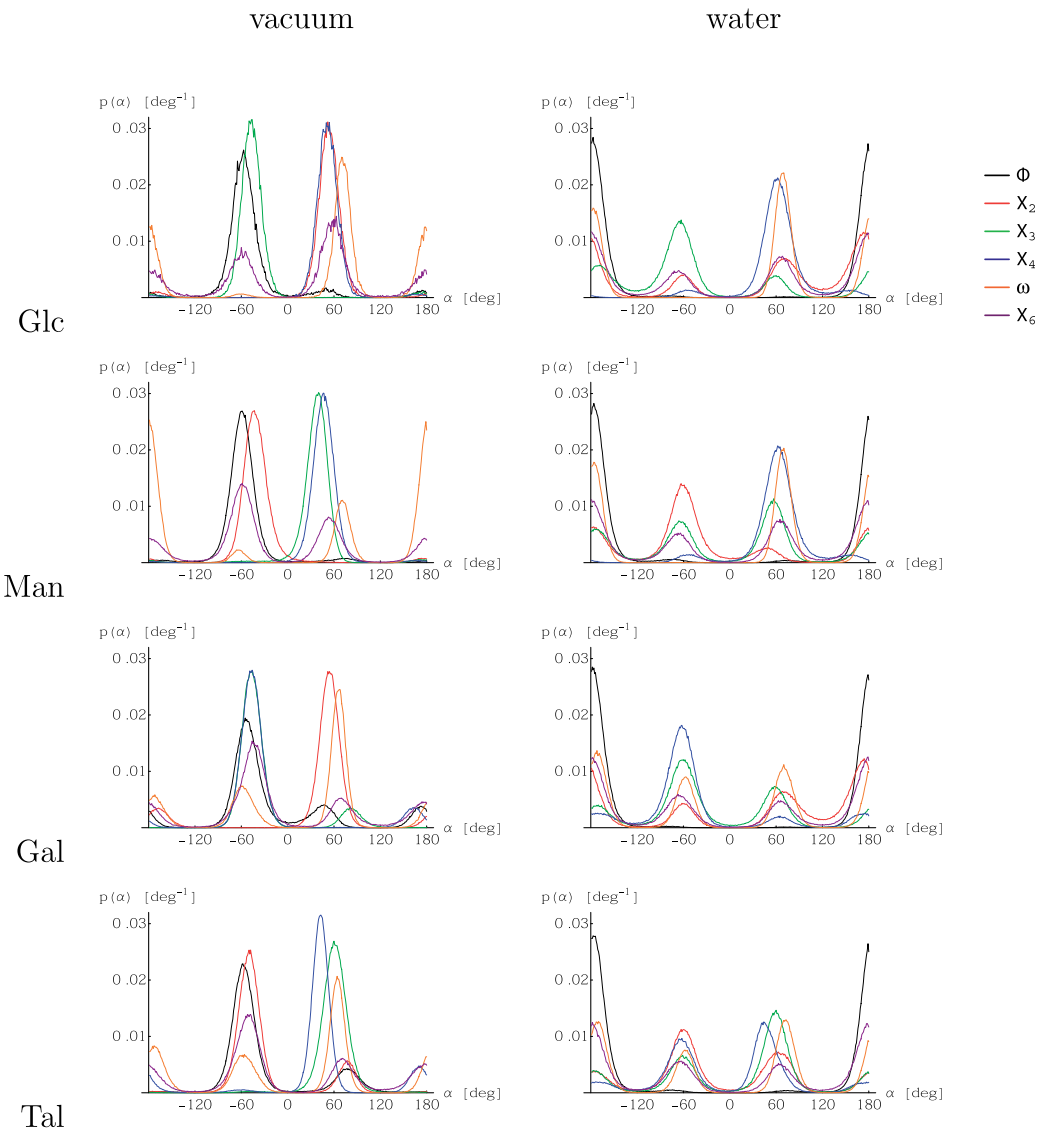

Figure 2. Normalized probability distributions associated with the six exocyclic dihedral angles ϕ, χ_n ($n = 2,3,4,6$) and ω as obtained from 200 ns simulations of Glc, Man, Gal and Tal (Fig. 1) in vacuum (SD; left) or in water (MD; right). The corresponding integrated populations for the three staggered rotamers are reported in Table 2.

membered 'rings'; data not shown). For intramolecular hydrogen-bonds, average lifetimes were also estimated using an allowed excursion time of 1 ps (required delay before considering a given hydrogen-bond to be broken).

The dynamics of exocyclic dihedral angles was investigated by monitoring transitions between the g_+, t and g_- wells with an allowed excursion time of 1 ps (i.e., a transition between two wells is recorded if the dihedral angle spent at least 1 ps in the first well followed by at least 1 ps in the second well).

The solvation structure was analyzed by calculating time-averaged and spatially resolved atom number densities.[195,277,296–298,300,301,306] These were obtained by placing the solute in its initial configuration at the center of a cube of edge length 1.5 nm spanned by a three-dimensional cubic grid with 100 grid points along each dimension. Successive configurations along the trajectory were superimposed onto this initial configuration by means of a roto-translational least-squares fit[322] based on the sugar heavy atoms (excluding O_6). The number of occurrences of each atom type (solute and solvent) in each grid cell was then averaged over time and visualized in the form of number density isosurfaces using the program PYMOL.[323]

All analysis programs were implemented in Jython and Mathematica as extensions to the open-source molecular mechanics analysis package ESRA.[324]

3. Results and discussion

3.1. Ring conformation

In water, three of the four hexopyranoses considered, Glc being the exception, remained in the $^4C_1$ chair conformation during more than 99.9% of the simulation time. The $^4C_4$ chair conformation was not observed in any simulation. For Glc, alternative ring conformations were encountered in about 0.7% of the sampled configurations, including 0.2% of a $^{3,0}B$ boat (the remaining 0.5% are twisted conformations, neither chair nor boat). The $^{3,0}B$ conformation appeared in 16 distinct events along the 200 ns simulation, with lifetimes comprised between 10 and 100 ps. For hexopyranoses with an equatorial 3-OH group in the $^4C_1$ conformation (all compounds considered here), this $^{3,0}B$ conformation may be stabilized by intramolecular hydrogen-bonding between this group and the ring oxygen. A similar behavior was found in vacuum, where Man, Gal and Tal remained in the $^4C_1$ chair conformation during more than 99.9% of the simulation time, while the $^{3,0}B$ boat conformation presented an occurrence of 0.4% for Glc.

Experimentally, the aldohexopyranoses of the D-series are known to predominantly adopt the $^4C_1$ chair conformation (Section 1). However, a $^1C_4$ conformation appears to be significantly populated for the α- and (to a lesser extent) β-anomers of D-idose (populations ~80% and ~25% for the α- and β-anomers, respectively[30]), as well as D-altrose and (possibly) D-gulose (population ratios unknown). This alternative chair conformation may become dominant for some D-monosaccharide derivatives (e.g., of glucose,[194,325] idose,[59,83,326] xylose[327] and iduronates[48,51,54,57,58,60,328]).

Most (empirical or theoretical) estimates suggest a stability difference comprised between 25 and 45 kJ mol^{-1} between the two chair conformations of Glc in the gas-phase.[18,49,50,77–81] Recent quantum-mechanical calculations also indicate the existence of boat and skew-boat conformers within 17–40 kJ mol^{-1} of the $^4C_1$ conformation, with an estimate of 27 kJ mol^{-1} for the lowest boat conformer.[81]

Experimentally, boat conformations have been observed in Glc derivatives (both in the solid state[329] and in solution[53,63,330]), and are probably involved in single-molecule force spectroscopy experiments on amylose.[331] Their transient formation in aqueous solution has been suggested by ultrasonic-relaxation spectroscopy measurements[36,86–88] to occur with characteristic timescales of the order of 50–150 ns. The timescale of about 10 ns associated with chair–boat interconversions in the present simulation of Glc is thus of a reasonable order of magnitude.

Even if the relatively large energy differences estimated by quantum-mechanical calculations in vacuum are somewhat attenuated by solvation effects, it seems unlikely that alternative chair or boat conformers are significantly populated in aqueous solutions of Glc, where they could in principle be detected by NMR methods with a sensitivity of at least a fraction of a percent.[24] However, to our knowledge, only one study[82] explicitly reported the absence of the $^1C_4$ chair conformation for aqueous Glc (with a quoted uncertainty of about 2%), while no experimental work to date has directly aimed at measuring the equilibrium populations of boat conformers. Therefore, the observation of such conformers in the simulations is not strictly incompatible with experimental data, the presently observed occurrence of 0.2% for the $^{3,0}B$ conformation of Glc corresponding to a free-energy of about 15.5 kJ mol^{-1} relative to the $^4C_1$ conformation (the corresponding intramolecular energy difference has been previously estimated[265] to 20.4 kJ mol^{-1}).

Nevertheless, the appearance of boat conformers during the simulations (as well as the distinct flexibility of Glc compared to the three other hexopyranoses) may also result from a minor deficiency of the force field[265] employed in terms of ring torsional potentials. Although some authors have solved this 'problem' by artificially locking the conformation of the ring in $^4C_1$ using additional 'unphysical' force field terms,[264,284,285] this does not represent a generally applicable strategy for an

all-purpose carbohydrate force field, and a reoptimization of the ring torsional potentials used in GROMOS 45A4 is currently in progress.

3.2. Intramolecular hydrogen-bonding

The occurrences of intramolecular hydrogen-bonds during the simulations of the four hexopyranoses, both in vacuum and in water, are reported in Table 1. Note that within the GROMOS force field,[258,259] hydrogen-bonding interactions only result from attractive electrostatic interactions between point charges on the donor, hydrogen and acceptor atoms, balanced by van der Waals (Lennard-Jones) repulsion between the donor and acceptor atoms. No specific hydrogen-bonding force field term is applied, but a special set of repulsive Lennard-Jones parameters is selected for potentially hydrogen-bonding donor–acceptor pairs.

In the context of the four aldohexopyranoses considered in the present study (β-anomers), one can distinguish four types of hydrogen-bonds (in order of decreasing expected strength; Section 1): (i) six-membered hydrogen-bonded 'rings' involving the 1,3-*syn*-diaxial 2-OH and 4-OH groups of Tal (either $H_2 \rightarrow O_4$ or $H_4 \rightarrow O_2$), or the 6-OH (hydroxymethyl) and 4-OH groups in the four compounds (either $H_4 \rightarrow O_6$ or $H_6 \rightarrow O_4$; possible with ω in g_- for Glc and Man, or in g_+ for Gal and Tal); (ii) five-membered hydrogen-bonded 'rings' between cis-vicinal (axial–equatorial) hydroxyl groups (i.e., involving the 2-OH group of Man and Tal, or the 4-OH group of Gal and Tal); (iii) five-membered hydrogen-bonded 'rings' between trans-vicinal (diequatorial) hydroxyl groups; and (iv) five-membered hydrogen-bonded 'rings' involving the 6-OH (hydroxymethyl) group and the ring oxygen ($H_6 \rightarrow O_5$; possible with ω in g_+ or t). Hydrogen-bonds of the three

Table 1. Occurrences of intramolecular hydrogen-bonds as obtained from 200 ns simulations of Glc, Man, Gal and Tal (Fig. 1) in vacuum (SD; left) or in water (MD; right)

H	*O*	Vacuum				Water			
		$\langle d \rangle$ (nm)	$\langle \alpha \rangle$ (°)	Occ. (%)	τ (ps)	$\langle d \rangle$ (nm)	$\langle \alpha \rangle$ (°)	Occ. (%)	τ (ps)
Glc									
1	2					0.24	107	15	<0.5
2	1	0.23	110	48	1.8				
2	3					0.24	108	11	0.6
3	2	0.23	112	71	7.0	0.23	108	13	0.6
3	4					0.23	107	6	0.6
4	3	0.23	111	69	5.5	0.23	108	29	1.0
6	5	0.23	108	20	0.5				
Man									
2	1	0.23	112	53	2.9	0.24	109	12	<0.5
3	2	0.23	113	71	7.7	0.23	110	10	0.6
3	4					0.23	108	8	0.9
4	3	0.23	111	74	8.8	0.23	109	28	1.0
6	5	0.23	108	22	0.6				
Gal									
1	2	0.23	111	7	3.3	0.24	107	14	<0.5
2	1	0.23	110	38	1.4				
2	3	0.23	111	6	2.6	0.24	109	9	0.5
3	2	0.23	112	61	5.4	0.24	109	12	0.6
3	4	0.22	112	8	11.5				
4	3	0.23	110	53	4.2	0.24	108	12	<0.5
4	6	0.20	137	11	10.5	0.20	135	8	3.6
6	4	0.20	136	47	11.2	0.21	131	5	2.5
Tal									
1	2	0.23	111	10	2.7				
2	1	0.23	111	41	2.2	0.24	109	10	<0.5
2	4	0.20	138	16	66.0	0.21	133	21	3.2
3	2	0.24	109	11	<0.5	0.24	109	5	<0.5
3	4	0.24	108	11	<0.5				
4	2	0.19	140	82	275.8	0.20	137	40	9.0
4	6	0.20	133	13	40.9	0.20	134	6	2.8
6	4	0.21	133	36	7.9	0.21	130	5	2.5

The corresponding donor hydrogen (*H*), acceptor oxygen (*O*), average hydrogen–acceptor distance ($\langle d \rangle$), average donor–hydrogen–acceptor angle ($\langle \alpha \rangle$), occurrence along the trajectory (occ.), and average lifetime (τ) are listed. Only hydrogen-bonds occurring in at least 5% of the configurations are reported. The lifetimes are calculated using an allowed excursion time of 1 ps. Values below 0.5 ps (writing frequency of the successive configurations along the trajectories) cannot be quantified (<0.5 ps). Hydrogen-bonding criterion: maximum hydrogen–acceptor distance of 0.25 nm, minimum donor–hydrogen–acceptor angle of 100°.

latter types are characterized in the simulations by average donor–hydrogen–acceptor angles close to 110° (Table 1), and should probably rather be viewed as favorable hydrogen–oxygen electrostatic interactions. The term hydrogen-bond will nevertheless be retained here in a loose sense.

In the gas-phase simulations, a persistent counterclockwise (as viewed from the β-side of the ring) hydrogen-bond network is found for all hexopyranoses considered (pattern 4→3→2→1 for Glc, Man and Gal; pattern 4→2→1 for Tal). These hydrogen-bonds have occurrences of 38–82%. Additionally, when the 4-OH group is equatorial (Glc, Man), a $H_6 \rightarrow O_5$ hydrogen-bond is observed (occurrence about 20%). When this group is axial (Gal, Tal), a $H_6 \rightarrow O_4$ hydrogen-bond is observed instead (occurrence about 40%; together with a minor contribution of $H_4 \rightarrow O_6$). No systematic differences can be observed between the occurrences of hydrogen-bonds involving cis- and trans-vicinal hydroxyl groups.

For Glc, a counterclockwise 4→3→2→1 network along with a clockwise $H_6 \rightarrow O_5$ hydrogen-bond was also found in the lowest-energy conformer by most quantum-mechanical studies of Glc or its O_1-methylated derivative in vacuum[79–81,104,255,332–340] (although some studies[23,341] suggested a $H_6 \rightarrow O_4$ hydrogen-bond instead). This observation also agrees with the results of IR ion-dip experiments on phenyl-β-D-glucopyranoside in the gas phase.[162,163,338] For Man the available quantum-mechanical results[255,337,342] also suggest a counterclockwise network in the lowest-energy conformer, but along with a $H_6 \rightarrow O_4$ hydrogen-bond. The same counterclockwise network was also found in previous quantum-mechanical calculations on Gal or its O_1-methylated derivative in vacuum,[104,162,163,255,337,340,343–346] although most of these calculations (see, however[104,343]) as well as IR ion-dip experiments on phenyl-β-D-galactopyranoside in the gas-phase[162,163,344] suggested the presence of a $H_6 \rightarrow O_5$ hydrogen-bond (as in Glc) rather than a $H_6 \rightarrow O_4$ hydrogen-bond (present simulation) in the lowest-energy conformer. Finally, for Tal, the only quantum-mechanical study available to our knowledge also supports the presence of a $H_6 \rightarrow O_5$ hydrogen-bond.[337]

The stability of a hydrogen-bond network (over individual uncorrelated hydrogen-bonds) is certainly a consequence of cooperativity effects (Section 1). The observed preference for a counterclockwise orientation in the four compounds considered (which may not be generalizable to the corresponding α-anomers as well as to other hexopyranoses[162,255,340,345]) is probably related to its compatibility with the g_- preference of ϕ for β-anomers in the gas-phase (*exo*-anomeric effect; Section 3.3 and Table 2).

In the gas-phase simulations, a hydrogen-bond between the 1,3-*syn*-diaxial 2-OH and 4-OH groups of Tal is present (in one direction or the other, with a strong predominance of $H_4 \rightarrow O_2$) during 98% of the simulation time. This agrees with the expected high strength of six-membered hydrogen-bonded 'rings' involving 1,3-*syn*-diaxial hydroxyl groups in fixed relative orientations,[110,114,141,148,156] which has been clearly evidenced in model compounds by quantum-mechanical calculations in vacuum[154] and by NMR[122,146] and IR[150] spectroscopy experiments in nonpolar solvents. The same hydrogen-bond is also found in the crystallographic structure of α-D-talopyranose.[347]

A similar six-membered 'ring' hydrogen-bond is also possible between the 6-OH (hydroxymethyl) and 4-OH groups. However, these two groups are not in fixed relative orientations and hydrogen-bonding requires the freezing of one rotatable *C*–*C* bond (C_5–C_6), namely ω

Table 2. Relative populations of the three staggered conformers of the six exocyclic dihedral angles ϕ, χ_n ($n = 2,3,4,6$) and ω, as obtained from 200 ns simulations of Glc, Man, Gal and Tal (Fig. 1) in vacuum (SD) or in water (MD)

(%)	Vacuum			Water			Vacuum			Water		
	g_+	t	g_-	g_+	t	g_-	g_+	t	g_-	g_+	t	g_-
	Glc						Man					
ϕ	5	4	91	1	98	2	4	2	94	2	96	3
χ_2	97	3	0	33	52	14	2	2	96	12	27	61
χ_3	0	3	97	14	27	59	95	2	3	42	27	31
χ_4	97	3	0	89	6	5	98	2	0	88	6	6
ω	63	35	2	57	43	0	28	67	5	52	48	0
χ_6	49	21	30	30	50	20	30	18	52	30	48	22
	Gal						Tal					
ϕ	16	12	72	1	98	1	18	2	80	2	96	2
χ_2	88	12	0	31	53	16	16	1	83	34	18	48
χ_3	11	0	88	29	17	54	98	1	1	56	17	28
χ_4	0	11	88	8	17	75	83	15	2	47	12	41
ω	57	17	25	33	41	26	49	26	25	39	39	22
χ_6	21	20	59	20	54	26	23	23	54	22	53	26

The corresponding probability distributions are displayed in Figure 2.

in g_- for Glc and Man, or in g_+ for Gal and Tal. Restricting the analysis to configurations involving these specific ω-rotamers, the hydrogen-bond is found to be formed nearly systematically (data not shown). However, the occurrences of these rotamers are very small ($\leqslant$5%) for Glc and Man, and are limited (50–60%) for Gal and Tal (Section 3.3 and Table 2). Therefore, it appears that even in vacuum, the formation of a (six-membered 'ring', i.e., relatively strong) hydrogen-bond between the 6-OH and 4-OH groups represents a limited conformational driving force in determining the hydroxymethyl group orientation. Similar considerations apply to the (five-membered 'ring', that is, comparatively weaker) hydrogen-bond involving the 6-OH group and the ring oxygen. However, in this case, the occurrence of the hydrogen-bond remains low ($\leqslant$25%), even when restricing the hydrogen-bond analysis to the g_+ and t rotamers of ω (data not shown).

Most of the hydrogen-bonds encountered in these gas-phase simulations have lifetimes of the order of 0.5-10 ps or below. However, the $H_4 \rightarrow O_2$, $H_2 \rightarrow O_4$ and $H_4 \rightarrow O_6$ hydrogen-bonds in Tal have significantly longer lifetimes.

In the water simulations, intramolecular hydrogen-bonds are frequent, but their occurrences never exceed 40% (or 29% if one excepts $H_4 \rightarrow O_2$ in Tal). This reduction in their occurrences may be dominantly attributed to the solvent-induced dielectric screening of intramolecular electrostatic interactions (Section 1). The oriented hydrogen-bond networks encountered in vacuum partly persist in solution, in the form of (weak) preferences. However, there are two notable differences: (i) the hydroxymethyl group is no longer involved in any significant intramolecular hydrogen-bonding ($H_6 \rightarrow O_4$ and $H_4 \rightarrow O_6$ hydrogen-bonds are present in Gal and Tal, but with occurrences of at most 8%); (ii) $H_2 \rightarrow O_1$ hydrogen-bonds are no longer encountered when the 2-OH group is equatorial (Glc, Gal), in which case $H_1 \rightarrow O_2$ hydrogen-bonds occur instead. A high-occurrence hydrogen-bond persists between the 1,3-*syn*-diaxial 2-OH and 4-OH groups in Tal (in one direction or the other, with a predominance of $H_4 \rightarrow O_2$, during 61% of the simulation time). As was the case in vacuum, no systematic differences can be observed between the occurrences of hydrogen-bonds involving cis- and trans-vicinal hydroxyl groups.

Most of the observed hydrogen-bonds are quite labile, with an average lifetime of the order of 0.5–1.0 ps or below. However, the (low-occurrence) hydrogen-bonds involving the hydroxymethyl group in Gal and Tal have slightly longer lifetimes of about 3 ps, while the $H_4 \rightarrow O_2$ and $H_2 \rightarrow O_4$ hydrogen-bonds in Tal have lifetimes of 9.0 and 3.2 ps, respectively. Note that the present lifetimes, defined on the basis of a simple geometrical hydrogen-bonding criterion, should probably be viewed as lower bounds.[299]

Experimentally, NMR measurements of isotope effects on a series of monosaccharides in aqueous solution revealed a peculiar behavior for Tal, which was attributed to the presence of a hydrogen-bond between the 2-OH and 4-OH groups.[141] The observations were compatible with a hydrogen-bond of fixed directionality or in rapid flip-flop between the two possible orientations (similar observations were also made for a closely related inositol derivative in DMSO[146]). The present simulations support the second hypothesis, with a flip-flop on the 1–10 ps timescale.

3.3. Conformation of the exocyclic dihedral angles

The probability distributions associated with the six exocyclic dihedral angles ϕ, χ_n ($n = 2,3,4,6$) and ω during the simulations of the four hexopyranoses in vacuum as well as in water (Fig. 2) only display population peaks in the ranges corresponding to staggered conformations. The populations of eclipsed conformations at $-120°$, $0°$ and $120°$ are in all cases essentially negligible, so that it is sufficient for most purposes to consider the integrated populations of the three staggered rotamers (Table 2).

In the gas-phase simulations, the dihedral angle ϕ is nearly always found in the g_- conformation, a behavior consistent with the *exo*-anomeric effect (Section 1) for β-anomers, and explicitly accounted for by the torsional parameters of the carbohydrate force field used in the present study.[265] This effect results (in β-hexopyranoses) from (i) a favorable dipole–dipole interaction (the interaction between the bond dipoles of the C_1–O_5 and O_1–H_1 bonds is most favorable in the g_+ and g_- conformations); (ii) a hyperconjugative effect (the overlap between the nonbonding n-orbitals on O_1 and the antibonding σ^*-orbital of the C_1–O_5 bond is largest in the g_+ and g_- conformations); and (iii) a steric effect (repulsion between the substituent at O_1, here H_1, and the substituents of the C_2 carbon, destabilizing the t and g_+ conformations).

In the water simulations, however, this dihedral angle is nearly always found in the t conformation (compatible with the occurrence of a $H_1 \rightarrow O_2$ hydrogen-bond during the simulations of Glc and Gal in water; Section 3.2). This observation contrasts with the vacuum results, but also with the preferred g_- orientation found in water and in crystals (both experimentally and in simulations) for β-linked disaccharides,[257,265,266,302] as well as for methyl-β-D-glucopyranoside (10 ns simulation with the present force field; data not shown). This apparent discrepancy can tentatively be rationalized by (*i*) a general weakening of the *exo*-anomeric effect upon going from vacuum to aqueous environment (solvent-induced dielectric screening); (ii) a specific weakening of the steric contribution to this effect in the presence of an unfunctionalized lactol group; (iii) a peculiar solvent structuring pattern involving the ring oxygen, the

unfunctionalized lactol group and at least two water molecules (Section 3.6). A weakening of the *exo*-anomeric preference in aqueous environment for an unfunctionalized lactol group was also observed in previous quantum-mechanical calculations using implicit-solvent models.[176,333] However, the observed inversion in rotameric stability is still to be taken with some caution, because (i) it has not been reported in previous MD simulations of β-hexopyranoses; (ii) the torsional potential used for ϕ in the present force field has been optimized for O_1-methylated compounds[265] rather than reducing hexopyranoses.

In the gas-phase simulations, the exocyclic dihedral angles χ_2, χ_3 and χ_4 almost exclusively adopt one of the two *gauche* conformations. These preferences depend on the hexopyranose considered, and correspond to the orientations compatible with the (strong) hydrogen-bond networks discussed previously (Section 3.2).

In the water simulations, hydrogen-bonding interactions are substantially weakened and the dihedral angles χ_2 and χ_3 present significant populations (>10%) in all three conformers. These two dihedral angles show a slight preference for *t* and g_-, respectively, when the 2-OH group is equatorial (Glc, Gal), and for g_- and g_+, respectively, when this group is axial (Man, Tal). These preferences are in line with the vacuum preferences except for χ_2 in Glc and Gal, where the leading conformer is g_+ in vacuum (compatible with a $H_2{\rightarrow}O_1$ hydrogen-bond; Table 1) but *t* in water (compatible with $H_1{\rightarrow}O_2$).

The orientational preferences around χ_4 are more pronounced. When the 4-OH group is equatorial (Glc, Man), χ_4 is almost exclusively found in the g_+ conformation (as in vacuum). When this group is axial (Gal, Tal), the distribution depends on the configuration of the 2-OH group. In Gal, where the latter group is equatorial, the g_- configuration is dominant (as in vacuum). In Tal, where this group is also axial, the three wells are populated, with a clear preference for g_+ (dominant in vacuum) and g_-. The g_+ conformation of χ_4 together with a g_- conformation of χ_2 is required for the formation of an intramolecular $H_4{\rightarrow}O_2$ hydrogen-bond (82% and 40% occurrences in vacuum and water, respectively; Table 1). The formation of a $H_2{\rightarrow}O_4$ hydrogen-bond (16% and 21% occurrences, respectively) requires χ_4 in *t* and χ_2 in g_+, which is less frequent.

In the gas-phase simulations, the dihedral angle ω shows preferences $g_+ > t$ for Glc and $t > g_+$ for Man, with nearly zero population for the g_- conformer. The absence of the g_- rotamer is probably in part due to the *gauche*-effect (Section 1), explicitly accounted for by the torsional parameters of the carbohydrate force field used in the present study.[265] In addition, the leading g_+ and *t* conformations correspond to two alternative ways of forming a $H_6{\rightarrow}O_5$ hydrogen-bond (Table 1), from either above (g_+; with χ_6 in g_+) or below (*t*; with χ_6 in g_-) the ring plane. However, this (weak) hydrogen-bond only has an occurrence of about 20% for the two compounds. Although the g_- conformer could in principle also form 1,3-*syn*-diaxial $H_6{\rightarrow}O_4$ or $H_4{\rightarrow}O_6$ hydrogen-bonds with the equatorial 4-OH group, neither these hydrogen-bonds nor the g_- conformer are significantly populated. These observations suggest again that hydrogen-bonding is not a major conformational driving force in determining the orientation of the hydroxymethyl group, even in vacuum (Section 3.2).

For Glc, the above conformational preferences agree well with the results of most quantum-mechanical calculations on Glc or its O_1-methylated derivative in vacuum, suggesting a stability ranking $g_+ > t > g_-$[79–81,104,162,163,255,334–336,338] (see, however[23,332,333,337,339–341]). The present observations are also compatible with the results of IR ion-dip experiments on phenyl-β-D-glucopyranoside in the gas-phase,[162,163,338] suggesting a population ratio $g_+/t/g_-$ of 25:68:7 (the inversion between g_+ and *t* may be related to the presence of the phenyl substituent[162,163,338,348]), as well as with Raman optical activity measurements on methyl-β-D-glucopyranoside in vacuum,[340] suggesting a corresponding approximate population ratio of 50:50:0. For Man, the few quantum-mechanical studies available suggest a ranking $g_- > t > g_+$.[255,337,342] However, such an inversion of relative rotamer stabilities compared to Glc (not observed in the present simulations) seems quite unlikely considering that the 2-OH and hydroxymethyl groups are situated at opposite sides of the ring and that the latter group is always equatorial.

The orientational preferences of ω for Gal and Tal as observed in the vacuum simulations are $g_+ > t \approx g_-$. The leading g_+ conformation permits the formation of a $H_6{\rightarrow}O_4$ (with χ_4 in g_- and χ_6 in g_-) or a $H_4{\rightarrow}O_6$ (with χ_4 in *t* and χ_6 in *t*) hydrogen-bond with the axial 4-OH group (Table 1). The preferences of χ_4 and χ_6 in Gal agree with the presence of a dominant $H_6{\rightarrow}O_4$ hydrogen-bond for this compound. The same hydrogen-bond is found with a slightly lower occurrence in Tal, although χ_4 is predominantly g_+ (due to the formation of the leading $H_4{\rightarrow}O_2$ hydrogen-bond) in this case (but with an average angle of about 45°; Fig. 2).

For Gal, the above preferences are at odds with the results of most quantum-mechanical calculations on Gal or its O_1-methylated derivative, suggesting a stability ranking $t \gg g_- > g_+$[162,163,255,337,340,344–346] (see however[104,343]), with experimental IR ion-dip studies on phenyl-β-D-galactopyranoside in the gas phase,[162,163,344] suggesting a population ratio $g_+/t/g_-$ of 0:90:10, and with Raman optical activity measurements on methyl-β-D-galactopyranoside in vacuum,[340] suggesting a corresponding approximate population ratio of 30:50:20. For Tal, the only quantum-mechanical study available to our knowledge suggests a ranking $t > g_- \gg g_+$.[337] The discrepancy between the vacuum simulation results

and the available quantum-mechanical and experimental data for Gal and Tal suggests the presence of a deficiency in the present force field[265] with respect to the torsional parameters for the ω dihedral angle in hexopyranoses with an axial 4-OH group (see below).

In the water simulations, the g_- conformer of ω is not populated when the 4-OH group is equatorial (Glc, Man), as was the case in vacuum, while the g_+ and t conformations now have nearly equal populations. These preferences are not significantly influenced by intramolecular hydrogen-bonding (the $H_6 \rightarrow O_5$ hydrogen-bond is absent in water, and the $H_6 \rightarrow O_4$ or $H_4 \rightarrow O_6$ hydrogen-bonds do not even occur in vacuum; Table 1). When the 4-OH group is axial (Gal, Tal), the three conformers of ω are almost equally populated (with a slight preference for g_+ and t). The decrease in the g_+ population compared to the vacuum simulations is probably caused by the solvent-induced weakening of the $H_6 \rightarrow O_4$ and $H_4 \rightarrow O_6$ hydrogen-bonds, which become nearly inexistent in water (Table 1). However, the limited magnitude of this decrease (24% and 10% for Gal and Tal, respectively) and the low-occurrence of these hydrogen-bonds in water hint again toward a quasi-negligible influence of hydrogen-bonding in determining the conformational preferences around ω in aqueous solution. For all hexopyranoses considered, the dihedral angle χ_6 presents significant populations (>20%) in all three conformers, with a systematic preference for t (6-OH group pointing away from the ring cycle).

The above observations can be compared with experimental data from NMR measurements on Glc, Man, Gal and their O_1-methylated derivatives in water (Table 3). For Glc and Man, all the available experimental data sets[93,95,96,98–104] support the quasi-absence of the g_- conformer for ω and suggest a population ratio $g_+/t/g_-$ of about 50:50:0 (see, however[93]), in good agreement with the present simulation results (57:43:0 for Glc and 52:48:0 for Man). This ratio is also compatible with vacuum-ultra-violet circular dichroism (VUVCD) data for Glc and Man,[349] and with the corresponding statistical preferences in the solid state for monosaccharide derivatives presenting the gluco configuration[130,350] (60:40:0). For Gal, the two most recent NMR studies[95,96] suggest a population ratio of about 5:70:25, while earlier measurements[93,100,102,104] support a ratio of about 20:55:25 (the differences arising mainly from the use of different Karplus equations). The present simulation results (33:41:26) are in better agreement with the latter set, as well as with VUVCD data for Gal.[349] However, the corresponding statistical preferences in the solid state for monosaccharide derivatives presenting the galacto configuration[130,350] (8:58:34) rather support the absence of the g_+ conformer. Thus, although the simulation results can be considered to agree well with the available experimental data for Glc and Man, the large uncertainty in the literature values for Gal renders the comparison difficult (beyond the observation that t is in all cases the leading conformer).

Table 3. Relative populations of the three staggered conformers of the hydroxymethyl group (dihedral angle ω), as obtained from 200 ns MD simulations of Glc, Man, Gal and Tal (Fig. 1) in water (sim) and as determined experimentally (Glc, Man and Gal only)

(%)	Ref.	g_+ (gg)	t (gt)	g_- (tg)
Glc	sim.	57	43	0
	a	53	45	2
	a (Me)	50	47	3
	c	49	49	2
	c (Me)	55	45	1
	c (Me)	48	50	2
	d	15	88	−3
	d (Me)	7	88	5
	e	45	62	−7
	f (Me)	50	62	−13
	g(Me)	41	52	7
	h (Me)	31	61	8
	i	31	59	10
Man	sim.	52	48	0
	b	48	49	3
	b (Me)	46	51	3
Gal	sim.	33	41	26
	a	22	53	25
	a (Me)	22	55	23
	c (Me)	17	59	24
	d	17	66	17
	f (Me)	29	53	18
	g(Me)	3	67	30
	h (Me)	3	72	25
Tal	sim.	39	39	22

The experimental data (listed from the earliest to the most recent study) are derived from NMR experiments by (a) Nishida et al.,[99,100] (b) Hori et al.,[105] (c) Abraham et al.,[101,102] (d) Tvaroška and Gajdoš,[93] (e) Brochier-Salon and Morin,[103] (f) Tvaroška et al.,[104] (g) Stenutz et al.,[95] (h) Thibaudeau et al.[96] and (i) Suzuki et al.[98] The reported data refer to the β-anomers only, and correspond to either the unfunctionalized compound or the corresponding O_1-methylated derivative (Me). The corresponding probability distributions from the MD simulations are displayed in Figure 2.

Only two NMR studies report estimates for the conformational distribution of the χ_6 dihedral angle.[95,96] This distribution appears to be only weakly correlated with that of the ω dihedral angle,[96] again providing a hint toward the limited conformational influence of intramolecular hydrogen-bonding in water. The first study[95] estimates the population of the t conformer of χ_6 to 11% and 28% in Glc and Gal, respectively. The second one[96] reports corresponding $g_+/t/g_-$ population ratios of 21:20:59 and 23:38:39, respectively. The simulation results agree qualitatively with these estimates in the sense that the three conformers are significantly populated. However, the dominance of the t conformer observed in the simulations is not found in the above experiments.

Different authors attribute the main driving force for the conformational preferences of the hydroxymethyl group dihedral angle ω in water (and other

polar solvents) to different effects: (i) the *gauche effect*,[102,131,189,190,351] stabilizing the t and g_+ conformations; (ii) the formation of a $H_6 \rightarrow O_5$ hydrogen-bond,[102,104,352] also stabilizing the t and g_+ conformations; (iii) the presence of 1,3-*syn*-diaxial repulsion between the 4-OH and 6-OH groups[102,131,189] (destabilizing g_- for Glc and g_+ for Gal); and (iv) specific solvent effects.[104,241,251,293–295,333,353] On the other hand, the limited impact of intramolecular hydrogen-bonding between the 4-OH and 6-OH groups in water on this conformational distribution has been clearly evidenced experimentally by (i) examining the influence of the solvent polarity on this distribution;[101,102,131,152,157,180,189,190,305,351] (ii) analyzing the correlation between the rotamer populations of the ω and χ_6 dihedral angles[96] (see above); and (ii) investigating hexopyranose analogs and model compounds lacking specific potential hydrogen-bonding groups.[92,101,102,104,131,144,152,189,190,305,351,354–357] Many of these studies also hint toward a negligible effect of $H_6 \rightarrow O_5$ hydrogen-bonding.

The different points mentioned above lead us to think that 1,3-*syn*-diaxial repulsion may be the key to understanding the conformational properties of the hydroxymethyl group in water (with *gauche* and solvation effects being secondary, and intramolecular hydrogen-bonding essentially negligible): (i) the g_- conformation in Glc and the g_+ conformation in Gal appear to be the least stable in vacuum (quantum-mechanical calculations and experiment); (ii) these conformations are essentially forbidden in the solid state;[130,350] and (iii) these conformations are nearly absent in aqueous solution (NMR measurements; accepting the result of the two most recent experimental determinations for Gal[95,96] as the correct one).

If this interpretation is correct, the present force field[265] appears to provide an accurate description for Glc (both in vacuum and in water; besides a possible marginal overstabilization of g_+ over t compared to the most recent experimental determinations for Glc[95,96,98,103,104]), but tends to significantly overstabilize the g_+ conformer (at the expense of the t conformer) for Gal (both in vacuum and in water). A reoptimization of the torsional parameters used in GROMOS 45A4 for the ω dihedral angle (at least in hexopyranoses with an axial 4-OH group) seems therefore to be required (work in progress). For comparison, the population ratios $g_+/t/g_-$ for Glc and Gal obtained with other commonly used force fields (see also[98,272]) are 66:33:1 and 4:75:21 (CHARMM/CSFF[241]), 49:45:6 and 11:62:27 (AMBER/GLYCAM[251]), 69:27:4 and 9:53:38 (OPLS-AA-SEI[256]), and 48:47:5 and 5:70:25 (GROMOS/Spieser[263]).

3.4. Correlation between the exocyclic dihedral angles

The correlations between the probability distributions associated with selected dihedral angle pairs during the simulations of the four hexopyranoses in water are shown in Figure 3. The graphs display the excess two-dimensional probability for the specific pair, relative to the ideal situation of an uncorrelated distribution (product of one-dimensional probability distributions for the two individual dihedral angles). Figure 3 summarizes the key results of a more detailed and systematic analysis (two-dimensional probability distributions and correlations for all dihedral angle pairs, for both the simulations in water and in the gas-phase; Supplementary data, Figs. S.1–S.16).

In water, significant correlations are exclusively found for the pairs χ_2–χ_3, χ_3–χ_4, χ_2–χ_4, χ_4–ω and ω–χ_6 (Fig. 3), as well as ϕ–χ_2 (Supplementary data, Figs. S.10, S.12, S.14 and S.16). Additional (weaker) correlations are seen for χ_3–ω and χ_4–χ_6 in Gal and Tal (Supplementary data, Figs. S.14 and S.16), as well as for ϕ–χ_4 and χ_2–ω in Tal (Supplementary data, Fig. S.16). In all cases, the areas of the two-dimensional maps indicating large positive correlations correspond to a subset of the areas with high probabilities (i.e., to well populated conformers; Supplementary data, Figs. S.9, S.11, S.13 and S.15). This is not surprising (but not trivial either) since a positive correlation between two hydroxyl groups in a given conformation is indicative of a favorable (e.g., hydrogen-bonding or dipole–dipole) interaction, which also acts to stabilize this specific conformation. Conversely, regions with large negative correlations usually (but not always) correspond to poorly populated conformers.

The correlation maps for χ_2–χ_3 in hexopyranoses where the 2-OH group is equatorial (Glc, Man) show positive correlations in the hydrogen-bonding conformations g_+–g_- ($H_3 \rightarrow O_2$) and t–t ($H_2 \rightarrow O_3$), in agreement with the hydrogen-bond analysis (Table 1), while they show a negative correlation in the t–g_- conformation (where the two hydroxyl groups point toward each other). These maps also reveal two interesting features about the interconversion between the two hydrogen-bonding conformers. First, among the four possible pathways for this interconversion (two conrotatory and two disrotatory), one appears to be clearly preferred. It is the disrotatory pathway involving a 60° change in the two dihedral angles. This pathway is probably favored over the three other ones because it is the shortest (in terms of dihedral angle variations) and benefits from favorable interactions between the antiparallel hydroxyl bond dipoles. Second, the rotations of χ_2 and χ_3 along this pathway are asynchronous. Close to g_+–g_- ($H_3 \rightarrow O_2$), χ_2 changes more rapidly than χ_3, while close to t–t ($H_2 \rightarrow O_3$), it is χ_3 that changes more rapidly. This feature is easily explained by the observation that hydrogen-bonding interactions impose more important orientational constraints on the donor hydroxyl group than on the acceptor one. The corresponding χ_2–χ_3 maps for hexopyranoses where the 2-OH group is axial

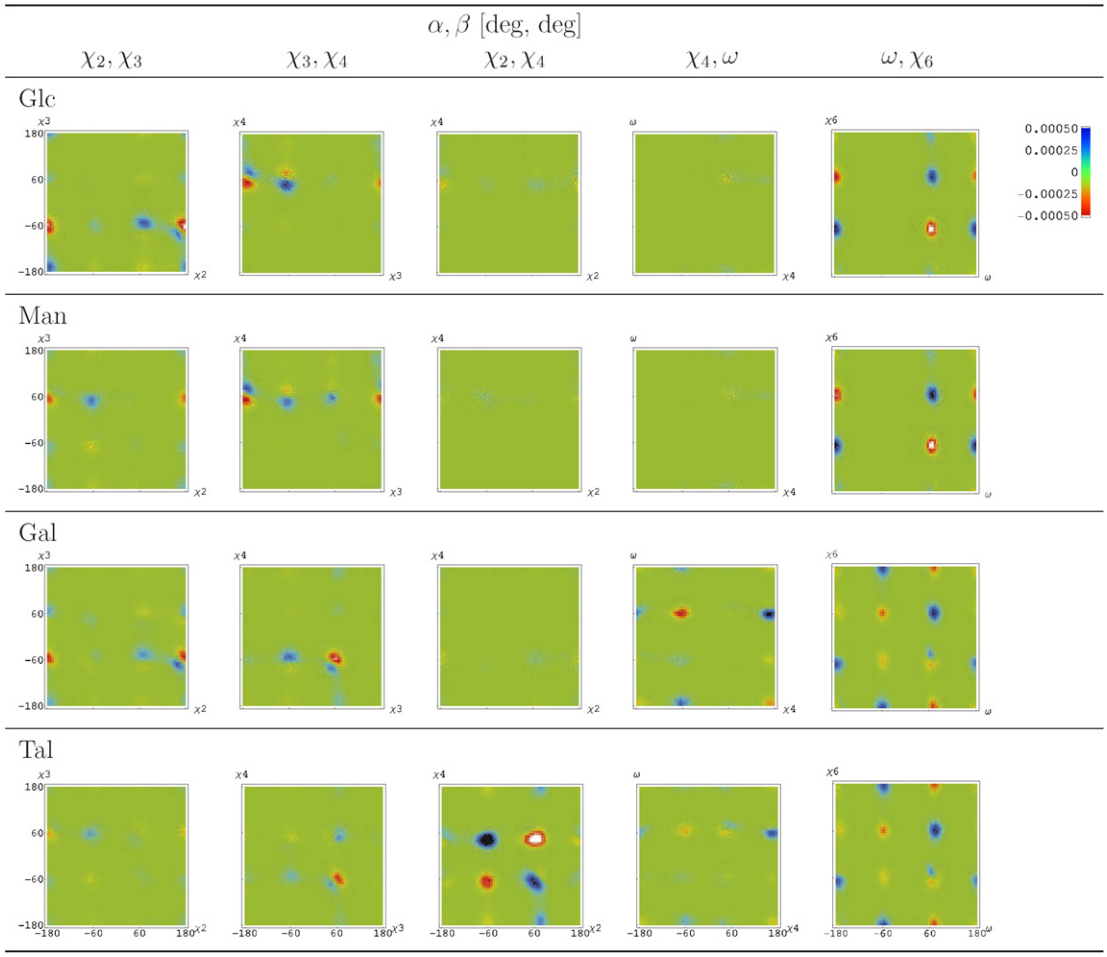

Figure 3. Correlation between the probability distributions associated with selected dihedral angle pairs α, β among ϕ, χ_n ($n = 2,3,4,6$), and ω, as obtained from 200 ns simulations of Glc, Man, Gal and Tal (Fig. 1) in water (MD). The correlation is measured by the excess probability $p(\alpha,\beta) - p(\alpha)p(\beta)$, where $p(\alpha,\beta)$ is the two-dimensional (normalized) probability distribution of the dihedral angle pair α,β, while $p(\alpha)$ and $p(\beta)$ are the corresponding one-dimensional (normalized) probability distributions for the two individual angles α and β. A more complete analysis of the two-dimensional probability distributions and corresponding correlations for both vacuum (SD) and water (MD) simulations is provided in Supplementary data, Figures S.1–S.16.

(Man, Tal) only show significant correlation for the hydrogen-bonding conformation g_-–g_+ ($H_3 \rightarrow O_2$) while the alternative hydrogen-bonding conformation t–t ($H_2 \rightarrow O_3$) is not significantly populated (Supplementary data, Figs. S.11 and S.15), in agreement with the hydrogen-bond analysis (Table 1).

Similar considerations apply to the χ_3–χ_4 maps, with positive correlations at g_-–g_+ ($H_4 \rightarrow O_3$) and t–t ($H_3 \rightarrow O_4$) for hexopyranoses where the 4-OH group is equatorial (Glc, Man), or g_-–g_- ($H_4 \rightarrow O_3$) and g_+–t ($H_3 \rightarrow O_4$) for hexopyranoses where this group is axial (Gal, Tal), and asynchronous disrotatory interconversion pathways between the two hydrogen-bonding conformers.

A significant correlation in the χ_2–χ_4 map is only found for Tal, where the axial configuration of the 2-OH and 4-OH groups permits the formation of a strong hydrogen-bond between the two groups (Section 3.2). Positive correlations are found for g_-–g_+ ($H_4 \rightarrow O_2$), g_+–g_- (only weakly hydrogen-bonding) and g_+–t ($H_2 \rightarrow O_4$), while a negative correlation is seen for g_+–g_+ (hydrogen atoms pointing at each other) and, to a lesser extent, g_-–g_- (hydrogen atoms pointing away from each other).

The χ_4–ω maps only show significant correlations for hexopyranoses where the 4-OH group is in axial orientation (Gal, Tal). Positive correlations are found for t–g_+ ($H_4 \rightarrow O_6$, if χ_6 in t) and g_-–t (non hydrogen-bonding), and negative ones for g_-–g_+ ($H_6 \rightarrow O_4$, if χ_6 in g_-). For t–g_+, we note that ω in g_+ correlates positively with χ_6 in g_+ rather than t (Fig. 3), suggesting that the $H_4 \rightarrow O_6$ hydrogen-bond is weak. For g_-–t, it is also seen that χ_4 in g_- and ω in t both correlate positively with χ_6 in g_-, offering the possibility of a $H_6 \rightarrow O_5$ hydrogen-bond from below the ring plane (Supplementary data, Figs. S.14 and S.16). However, this hydrogen-bond is not present with a significant occurrence in the water simulations (Table 1). Finally, for g_-–g_+, the conforma-

tion is well populated (Supplementary data, Figs. S.13 and S.15), although the correlation is negative. In this case, χ_4 in g_- correlates with χ_6 in g_- but ω in g_+ correlates with χ_6 in g_+, suggesting that the $H_6 \rightarrow O_4$ hydrogen-bond is also weak. For hexopyranoses where the 4-OH group is equatorial (Glc, Man), no significant correlations are seen on the χ_4–ω map.

The ϕ–χ_2 maps for the hexopyranoses where the 2-OH group is equatorial (Glc, Gal) show positive correlations for t–t ($H_1 \rightarrow O_2$) and t–g_+. The appearance of the latter conformation seems surprising at first sight, because the two hydrogen atoms point in the same direction. This particular conformation is actually stabilized by hydrogen-bonding to a common water molecule (Section 3.6). For hexopyranoses where the 2-OH group is axial (Man, Tal) positive correlations are found for t–g_- ($H_2 \rightarrow O_1$) and, to a lesser extent, for t–t and t–g_+. The two latter conformations do not allow for hydrogen-bonding, and the correlations are probably largely influenced by specific interactions with nearby solvent molecules.

For all hexopyranoses, the ω–χ_6 maps show positive correlations at t–g_- ($H_6 \rightarrow O_5$ hydrogen-bond from below the ring plane) and g_+–g_+ ($H_6 \rightarrow O_5$ hydrogen-bond from above the ring plane). For Gal and Tal, positive correlations are also seen for g_-–t (non hydrogen-bonding). For Glc and Man, negative correlations are seen for g_+–g_- (non hydrogen-bonding). The two latter observations are related to specific interactions with nearby solvent molecules (Section 3.6).

Such a correlation analysis has (to our knowledge) never been performed based on simulations of hexopyranoses. However, two-dimensional free-energy maps have been reported for the rotations around the analogs of ϕ–χ_2 and ω–χ_6 in model compounds, based on semi-empirical calculations with continuum solvation,[358] leading to results in good qualitative agreement with the present observations. Experimentally, although it has been shown that coupling constants between isotopically labelled adjacent ring carbon atoms are sensitive to the orientations of the two attached (vicinal) hydroxyl groups,[359] this observation has (to our knowledge) never been further exploited to gain information about hydroxyl group conformations and their correlations in solution. There is, however, an NMR study indicating that the correlation between the ω and χ_6 dihedral angles in Glc and Gal is weak,[96] thereby suggesting that the hydroxymethyl group is not involved in strong hydrogen-bonding interactions (neither with the 4-OH group nor with the ring oxygen; Sections 3.2 and 3.3).

3.5. Dynamics of the exocyclic dihedral angles

The timescales associated with the rotation around the various exocyclic dihedral angles during the simulations of the four hexopyranoses, both in vacuum and in water, are reported in Table 4. A more detailed analysis of the isomerization timescales associated with specific source and destination wells was also undertaken (Supplementary data, Tables S.I and S.II).

Table 4. Characteristic times τ associated with transitions of the six exocyclic dihedral angles ϕ, χ_n ($n = 2,3,4,6$) and ω as obtained from 200 ns simulations of Glc, Man, Gal and Tal (Fig. 1), in vacuum (SD) or in water (MD)

τ (ps)	ϕ	χ_2	χ_3	χ_4	ω	χ_6
Vacuum						
Glc	17	189	275	242	649	7
Man	40	42	31	146	647	8
Gal	6	388	226	215	122	8
Tal	28	108	70	101	107	6
Water						
Glc	85	11	13	24	813	17
Man	50	14	15	22	787	17
Gal	96	11	14	20	175	17
Tal	55	14	19	16	183	16

The characteristic times are obtained by dividing the total simulation time by the number of transitions between wells (g_-, g_+, t) observed for the dihedral angle during the simulation (with an allowed excursion time of 1 ps). A more complete analysis of well-to-well transition timescales is provided in Supplementary data, Tables S.I and S.II.

In vacuum, four main timescales can be distinguished for rotational isomerization: 6–8 ps for χ_6, 6–40 ps for ϕ, 31–388 ps for χ_n ($n = 2,3,4$) and ω in Gal and Tal, and 647–649 ps for ω in Glc and Man. These times should probably be regarded as lower bound estimates, due to enhanced sampling by application of SD rather than MD.

In water, four main timescales can be distinguished for rotational isomerization: 11–24 ps for χ_n ($n = 2,3,4,6$), 50–96 ps for ϕ, 175–183 ps for ω in Gal and Tal, and 787–813 ps for ω in Glc or Man. The slower timescale for rotation around ϕ compared to vacuum suggests that, just like the conformational preferences (Section 3.3), the dynamics of this dihedral angle in water is largely influenced by solvent effects (Section 3.6). The rotation around the χ_n dihedral angles is significantly faster than in vacuum (except for χ_6, where the change is limited), the corresponding timescales becoming very similar for all hydroxyl groups in the aqueous environment. This is certainly related to the weakening of hydrogen-bonding interactions by the solvent (Section 3.2), largely releasing the exocyclic hydroxyl groups from orientational constraints. The timescales for rotation around ω are comparable (only slightly longer) to the vacuum results, suggesting that the corresponding rotational barriers are dominated by intramolecular steric and stereoelectronic effects (included in the dihedral angle potential energy terms of the force field), and only weakly affected by intramolecular hydrogen-bonding and solvation.

The observation of a significantly (fourfold) slower relaxation for ω in Glc and Man (compared to Gal and Tal), and of a slightly faster relaxation for Man

(compared to Glc), is consistent with experimental trends from ultrasonic-relaxation spectroscopy measurements.[36,87,106] However, the corresponding experimental values (1.9, 1.7 and 0.6 ns for Glc, Man and Gal, respectively) are systematically higher by a factor of about 2.5 compared to the estimates of Table 4, which may be related to the overestimated diffusivity (underestimated viscosity) of the SPC water model employed in the present work.[315] Measurements of NMR relaxation times for lactose in DMSO also support a slower (factor about two) rotational diffusion of the hydroxymethyl group in the Glc compared to the Gal monomer.[360] The slower transition timescales for Glc and Man may be related to the quasi-absence of the g_- conformer of ω in these compounds, implying that four out of the six theoretically possible types of well-to-well transitions are essentially forbidden. However, even transitions between the t and g_+ wells are slowed down by about a factor of two compared to Gal and Tal (Supplementary data, Table S.II), suggesting that this difference in the dynamics is also due to intramolecular steric and stereoelectronic effects (included in the dihedral angle potential energy terms of the force field).

3.6. Solvation

The average numbers of solute–solvent hydrogen-bonds (per configuration) during the simulations of the four hexopyranoses in water are reported in Table 5. Each sugar molecule is involved in an average of 8.66–9.15 solute–solvent hydrogen-bonds. The hexopyranoses Glc, Man and Gal donate an average of 3.72, 3.74 and 3.80 hydrogen-bonds to water, while Tal donates only 3.43. The hexopyranoses Man, Gal and Tal accept an average of 5.25, 5.35 and 5.23 hydrogen-bonds from water, while Glc accepts only 5.06. As a result, Glc and Tal are involved in fewer solute–solvent hydrogen-bonds compared to Man and Gal. The above numbers may be compared to the corresponding averages of 0.73, 0.57, 0.54 and 0.83 for Glc, Man, Gal and Tal, respectively, for intramolecular hydrogen-bonds. As expected, hexopyranoses which form intramolecular hydrogen-bonds with higher-occurrences are found to form on average fewer solute–solvent hydrogen-bonds.[155,196] Considering all compounds, each hydroxyl group donates on average 0.73 hydrogen-bonds to water, and each oxygen atom (hydroxyl groups and O_5) accepts on average 0.87 hydrogen-bonds from water.

Table 5. Average numbers of solute–water hydrogen-bonds (per configuration) as obtained from 200 ns simulations of Glc, Man, Gal and Tal (Fig. 1) in water (MD)

	Glc	Man	Gal	Tal
HO_1	0.66	0.68	0.70	0.70
HO_2	0.70	0.69	0.75	0.64
HO_3	0.78	0.78	0.77	0.78
HO_4	0.84	0.85	0.83	0.59
HO_6	0.74	0.74	0.75	0.72
Subtotal	3.72	3.74	3.80	3.43
O_1	0.96	0.89	1.05	0.96
O_2	0.76	0.92	0.80	0.83
O_3	0.84	0.90	0.90	0.93
O_4	0.85	0.85	0.89	0.83
O_5	0.62	0.63	0.72	0.68
O_6	1.03	1.06	0.99	1.00
Subtotal	5.06	5.25	5.35	5.23
Total	8.78	8.99	9.15	8.66

The data are reported separately for hydrogen-bonds involving a solute hydroxyl group as donor (top; subtotal indicated) or a solute oxygen atom as acceptor (bottom; subtotal indicated). The overall total is also reported for each compound. Hydrogen-bonding criterion: maximum hydrogen–acceptor distance of 0.25 nm, minimum donor–hydrogen–acceptor angle of 100°.

The present estimates of about nine water molecules hydrogen-bonded to a hexopyranose agree qualitatively well with hydration numbers inferred from compressibility data[211] (8.4, 8.1, 8.7 and 7.7 for Glc, Man, Gal and Tal, respectively), and with NMR measurements on the hydroxyl protons, suggesting that each hydroxyl group is hydrogen-bonded to an average of two water molecules.[138,139] Note, however, that hydration numbers can be defined in many different ways[138,139,204,207,209,211] (probing distinct physical aspects of the solute–solvent interactions), leading to very different numerical values.

Based on the present simulation results (Table 5), the different hydroxyl groups can be approximately ranked in terms of donating propensity toward water as $HO_4 > HO_3 > HO_6 > HO_2 > HO_1$ and the different oxygen atoms in terms of accepting propensity as $O_6 > O_1 > O_3 > O_4 > O_2 > O_5$. These trends are essentially respected for all compounds, with the notable exception of the 4-OH group in Tal, the donating capacity of which is largely reduced by its involvement in a high-occurrence intramolecular hydrogen-bond ($H_4 \rightarrow O_2$, 40% occurrence; Table 1). The hydrogen-bonding propensities of the 2-OH and 4-OH groups are not obviously correlated with the equatorial vs axial orientation of the corresponding group (except for Tal), and no obvious preferential solvation of equatorial groups (as suggested by the axial–equatorial solvation model; Section 1) can be detected in the present simulations.

The weak accepting propensity of the ring oxygen is in line with the results of a survey of the Cambridge structure database, that failed to identify any crystallographic structure involving a hydrogen-bond between the ring oxygen and a water molecule.[361] On the other hand, the weak donating propensity of the lactol group is at odds with analyses of crystal structures and theoretical calculations suggesting that this group is a better hydrogen-bond donor and a poorer acceptor compared

Table 6. Occurrence of bridging water molecules as obtained from 200 ns simulations of Glc, Man, Gal and Tal (Fig. 1) in water (MD)

Bridge	Occ. (%)
Glc	
$HO_1::O::HO_2$	8
$HO_2::O::HO_3$	7
$HO_3::O::HO_4$	7
$O_3::HO::HO_4$	6
$O_1::H::O_5$	36
Man	
$HO_3::O::HO_4$	6
$O_3::HO::HO_4$	5
$O_1::H::O_5$	32
Gal	
$HO_3::O::HO_4$	5
$O_1::H::O_5$	42
Tal	
$HO_3::O::HO_4$	5
$O_1::H::O_5$	35

Only bridges occurring for at least 5% of the configurations are reported. Hydrogen-bonding criterion: maximum hydrogen–acceptor distance of 0.25 nm, minimum donor–hydrogen–acceptor angle of 100°.

to the other hydroxyl groups,[130,158–160,166,197] probably due to its increased acidity.

The possible presence of water molecules simultaneously hydrogen-bonded to two solute groups was also investigated in the simulations (Table 6). The most interesting observation is that a water molecule bridges the lactol (O_1) and ring (O_5) oxygen atoms for all hexopyranoses considered during 32–42% of the simulation time. The presence of this bridge probably explains at least in part the stability of the conformation with ϕ in t in the context of O_1-unsubstituted hexopyranoses (Section 3.3). As previously discussed, this conformation is disfavored by the *exo*-anomeric effect and essentially absent for O_1-substituted hexopyranoses (probably due to the steric repulsion between the O_1- and C_2-substituents). Other bridges are also observed, with significantly lower occurrences ($\leqslant$8%). The bridge between H_1 and H_2 in Glc may also explain the positive correlation observed for t–g_+ in the ϕ–χ_2 map (Section 3.3).

The structuring effect of the four hexopyranoses considered on the solvent is illustrated in Figure 4 in terms of three-dimensional density distributions for the different (solute and solvent) atoms in the system. All compounds exhibit similar features with respect to the solvation of the lactol group. A water molecule tends to bridge the ring (O_5) and lactol (O_1) oxygen atoms via a single hydrogen atom, while the lactol group (with ϕ almost exclusively in the t conformation) donates a hydrogen-bond to a tightly bound water molecule. Tightly bound water molecules are also found close to the 4-OH group for all hexopyranoses except Tal. For Glc and Man (4-OH group equatorial), the following observations apply: (i) O_4 tightly binds a water hydrogen atom located between O_4 and C_6; (ii) χ_4 is preferentially in g_+ (Table 2); (iii) H_4 tightly binds a water oxygen atom. It seems reasonable to suggest that the steric demands of C_6 effectively expel bulky water oxygen atoms from the region between C_6 and O_4, while a water hydrogen atom still fits in. The presence of this water hydrogen atom may in turn contribute to the observed conformational preference for χ_4 and the tight binding of a water molecule by H_4. The situation for Gal (4-OH group axial) is comparable to that encountered for Glc and Man (water hydrogen atom between O_4 and C_6, and water oxygen atom tightly bound to H_4), although χ_4 is here predominantly in the g_- conformation (Table 2) and the details of the coordination pattern differ somewhat. This coordination pattern is drastically weaker in Tal, probably due to the formation of the high-occurrence intramolecular $H_4 \rightarrow O_2$ hydrogen-bond in this compound (Section 3.2).

Interestingly, the two hydration sites mentioned above actually correspond to preferred water binding sites in the gas-phase monohydrates of phenyl-β-hexopyranosides as probed by IR ion-dip experiments.[162,348] A recent quantum-mechanical study of Glc monohydrates in vacuum[361] also suggested that the best water binding sites for Glc involved interactions with the O_5 and O_1 atoms, the 1-OH group systematically acting as donor for a strong sugar–water hydrogen-bond. The lowest-energy conformer not involving a direct interaction of the water molecule with the lactol group presented hydrogen-bonding interaction with the 4-OH group.

3.7. Relative stabilities

The free energies calculated for the six possible epimerization processes interconverting any two of the four hexopyranoses considered, both in vacuum (ΔG_{SD}) and in water (ΔG_{MD}), are reported in Table 7, together with the corresponding estimated changes in solvation free-energy ($\Delta G_{slv} = \Delta G_{MD} - \Delta G_{SD}$). Error bars are provided for these three quantities. Three sets of empirical estimates for the corresponding free-energy changes in aqueous solution are also reported (to be compared with ΔG_{MD}), as obtained through the Angyal scheme [18,21,67] (ΔG_A), or from molecular-mechanical calculations by Rao et al.[2,75] (ΔG_R) or using MM3[49] (ΔG_M).

The individual quantities ΔG_{MD} and ΔG_{SD} should be taken with some caution. Unlike some other classical force fields,[128,129,177,227–233] the GROMOS force field[258,265] has not been calibrated to reproduce molecular heats of formation (from either calorimetric measurements or quantum-mechanical calculations), because its main purpose is the description of (bio)physical processes (including solvation effects) rather than (bio)chemical ones. For this reason, its use is in general inappropriate for calculating overall free-energy changes involving a

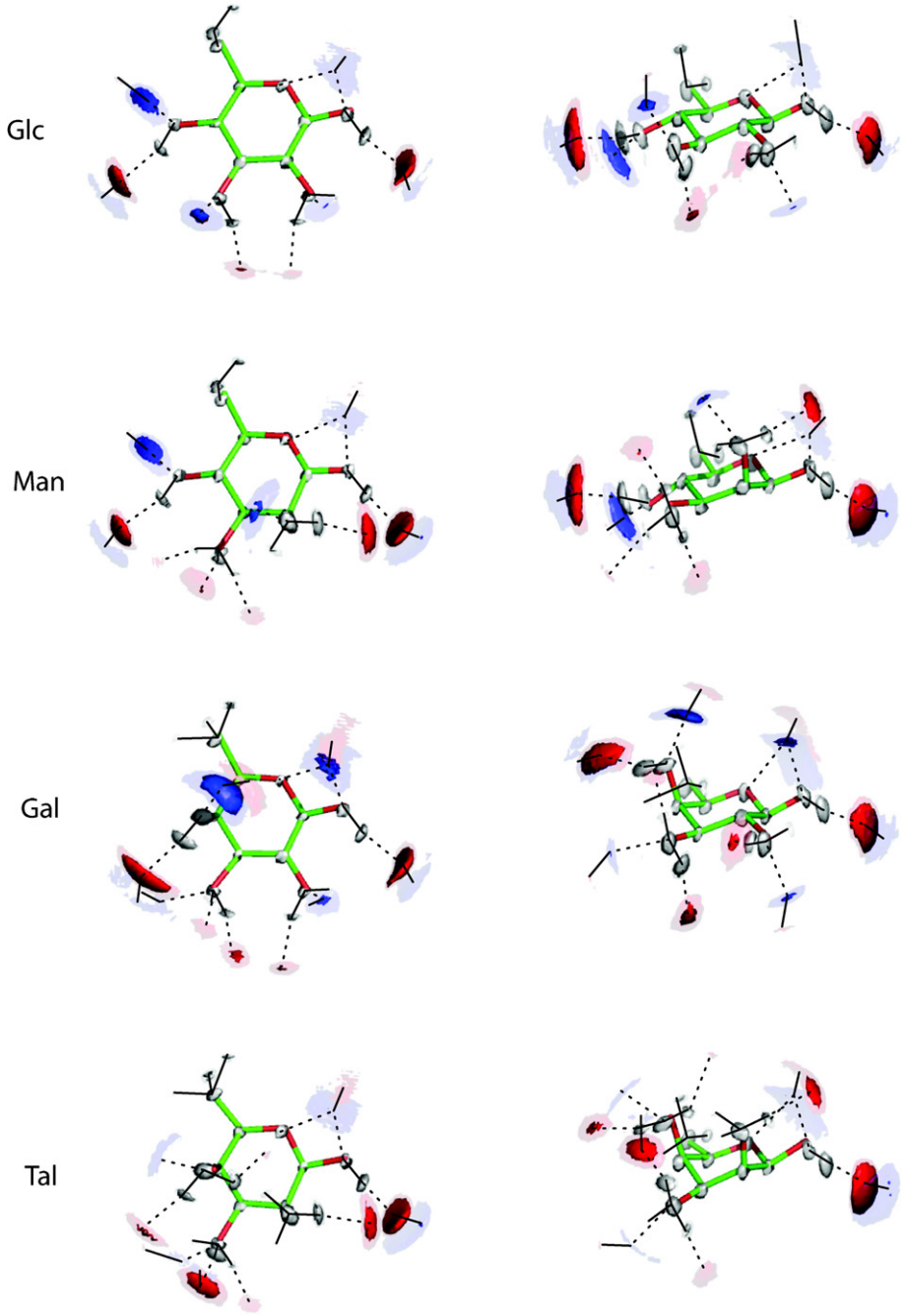

Figure 4. Number density isosurfaces of the solute (white), water oxygen (red) and the water hydrogen (blue) atoms, as obtained from 200 ns simulations of Glc, Man, Gal and Tal (Fig. 1) in water (MD). The sugar substructure (heavy atoms except O_6) used for the least-squares fitting of successive configurations is also drawn (sticks). Densities were calculated using a cubic volume of edge length 1.5 nm around the solute, spanned by a three-dimensional cubic grid with 100 grid points along each dimension. For each density, two isosurfaces are displayed: high density ρ_h (opaque) and low density $\rho_l = 0.7\rho_h$ (transparent), expressed in terms of the average number densities $\bar{\rho}$ of the corresponding atoms in the system, with $\rho_h = 600\bar{\rho}$ (solute atoms), or $\rho_h = 15\bar{\rho}$ (solvent atoms). Covalent bonds between high density spots are indicated with solid black lines (whenever identifiable). Hydrogen-bonds are indicated with dashed black lines (whenever identifiable; intra-solute hydrogen-bonds are omitted for clarity). Left: 'top' view, right: 'front' view.

change in the covalent structure of molecules. However, in the present case, all molecules considered share the same atom connectivity, the same nearest-neighbor non-bonded exclusion scheme, and nearly identical force field terms. The only differences[265] are changes in the signs of the reference improper-dihedral angles controlling the stereochemistries at C_2 and C_4, and a change in the form of the torsional potential associated with dihedral angle ω upon inversion of the stereochemistry at C_4. Due to this close similarity between the four com-

Table 7. Relative free energies of Glc, Man, Gal and Tal (Fig. 1) at 300 K as obtained from free-energy calculations in vacuum (SD) or in water (MD)

Transition	ΔG_A (kJ mol^{-1})	ΔG_R (kJ mol^{-1})	ΔG_M (kJ mol^{-1})	ΔG_{MD} (kJ mol^{-1})	ΔG_{SD} (kJ mol^{-1})	ΔG_{slv} (kJ mol^{-1})
Glc→Man	3.77	4.94	6.36	1.8 (1.8) ± 0.4	2.8 (2.6) ± 0.2	−1.1 (−0.8) ± 0.5
Glc→Gal	1.88	3.01	2.68	2.5 (2.5) ± 0.3	3.6 (3.7) ± 0.4	−1.2 (−1.2) ± 0.7
Glc→Tal	8.15	11.17	7.66	5.4 (5.2) ± 0.5	5.2 (5.4) ± 0.6	0.2 (−0.2) ± 1.1
Man→Gal	−1.88	−1.92	−3.68	0.6 (0.7) ± 0.5	1.1 (1.1) ± 0.4	−0.5 (−0.4) ± 0.9
Man→Tal	4.39	6.23	1.30	3.5 (3.4) ± 0.3	3.0 (2.8) ± 0.4	0.5 (0.6) ± 0.8
Gal→Tal	6.28	8.16	4.98	2.6 (2.7) ± 0.3	1.6 (1.7) ± 0.3	1.1 (1.0) ± 0.6
Cycle					Hysteresis (kJ mol^{-1})	
Glc→Man→Gal→Glc				0.1	0.3	0.3
Glc→Man→Tal→Glc				−0.1	0.6	0.8
Glc→Gal→Tal→Glc				0.4	−0.1	0.3
Man→Gal→Tal→Man				−0.3	−0.3	0.1

Top: free-energy changes upon epimerization calculated from MD simulations in water (ΔG_{MD}) and from SD simulations in vacuum (ΔG_{SD}), together with corresponding changes in the solvation free-energy ($\Delta G_{slv} = \Delta G_{MD} - \Delta G_{SD}$). Error bars based on block-averaging extrapolation[321] are also reported. The values in parentheses indicate free energies including minimal (least-squares-sum) corrections proportional to the estimated error and enforcing closure of all thermodynamic cycles. Three empirical estimates of the corresponding free-energy changes in aqueous solution are also provided (to be compared with ΔG_{MD}), as obtained for the β-anomer in the $^4C_1$ conformation according to the Angyal scheme[18,21,67] (ΔG_A), or from molecular-mechanical calculations by Rao et al.[2,75] (ΔG_R) or using MM3[49] (ΔG_M). Bottom: hysteresis of the thermodynamic cycles defined by combinations of the (uncorrected) free energies associated with the six epimerization processes (one of the four cycles is redundant).

pounds, the quantity ΔG_{MD} can probably be considered to be meaningful in the present context. The quantity ΔG_{SD}, however, may still fail to compare to the physical situation of hexopyranoses in vacuum, due to the use of effective force field parameters calibrated to reproduce properties in an aqueous environment (enhanced partial atomic charges). Note that these two issues only affect the individual quantities ΔG_{MD} and ΔG_{SD} but not their difference ΔG_{slv}, the accuracy of which is only limited by that of the interatomic forces within the force field employed (and the finite sampling).

The six epimerization free energies probe the relative stabilities of three hexopyranoses relative to a reference one and therefore contain redundant information. Thus, it is possible to check their internal consistency by assessing the closure of three thermodynamic cycles. The corresponding values are also reported in Table 7 (four cycles are selected for symmetry reasons, but each one is a linear combination of the three others). Both the error bars and the cycle-closure analysis suggest that the calculated free energies are remarkably precise (within the approximate molecular model employed), with uncertainties no larger than about 1 kJ mol^{-1}. By application of minimal (least-square-sum) corrections proportional to the corresponding estimated errors, cycle-closure can be enforced in the calculated epimerization free energies. The corresponding corrected values are indicated between parentheses in Table 7 (these will be considered as the best estimates of the present study and used as reference for the following discussion).

The results for ΔG_{MD} based on the simulations in water suggest a ranking Glc ≫ Man > Gal ≫ Tal in order of decreasing stability in aqueous solution, while the estimates from the three empirical schemes considered (ΔG_A, ΔG_R and ΔG_M) support a ranking Glc ≫ Gal ≫ Man ≫ Tal. The free-energy differences calculated using these empirical schemes are also generally of larger magnitudes compared to those estimated from the present simulations. Based on both the simulation results and on the empirical schemes, the inversion of the stereochemistry at either the C_2 or the C_4 carbon atom from equatorial to axial is associated with a raise in free-energy. In the case of the 2-OH group, this probably dominantly results from the introduction of a (steric) Δ2 repulsion (Section 1). The inversion in the relative stabilities of Man and Gal when comparing the results of the simulations and the three empirical schemes may be related to a possible deficiency in the description of compounds with an axial 4-OH group in the present force field (Section 3.3).

The above estimates of stability differences between epimers can be compared with a limited set of direct experimental results based on equilibrium epimer distributions. Enzyme-catalyzed epimerizations (through epimerases) almost exclusively involve phosphorylated sugars.[20,362] However, data exist for the enzymatic Glc→Man epimerization[363] (via fructose), with an estimated free-energy difference of 3.07 kJ mol^{-1}. Metal complexes can also catalyze epimerization at the C_2 carbon.[364–367] Focusing on studies where the obtension of an equilibrium C_2-epimer mixture was assessed, the free energies associated with the metal-catalyzed Glc→Man and Gal→Tal epimerization processes in water are estimated to be[364,365,367,368] 2.3–2.7 and[365,367,369] 3.0–3.4 kJ mol^{-1}, respectively. The present simulation estimates (ΔG_{MD}) of 1.8 and 2.7 kJ mol^{-1}, respectively, are in reasonable agreement with these numbers (although somewhat lower), while the values estimated

from the three other schemes tend to be significantly larger in magnitude. This comparison is of course only qualitative because (i) the epimerization experiments and the simulations are carried out under slightly different conditions (temperature, concentration, pH); (ii) the simulations only probe the epimerization free-energy for the β-anomers (rather than for the corresponding anomeric mixtures).

The results for ΔG_{SD} based on the simulations in vacuum lead to the same ranking of the four compounds as in water in terms of relative free energies, with values that are within at most 1.2 kJ mol^{-1} of ΔG_{MD}. This suggests that the leading contribution determining the relative stabilities of the different epimers is intramolecular in nature (primarily steric and stereoelectronic).

Although the impact of solvation on the relative free energies appears to be limited, it is nonnegligible. The trends in ΔG_{slv} suggest that the two hexopyranoses with equatorial–equatorial or axial–axial hydroxyl groups at C_2 and C_4 (Glc, Tal) are slightly less solvated (by about 1 kJ mol^{-1}) compared to the two hexopyranoses with axial–equatorial or equatorial–axial substitution (Man, Gal), with a ranking Gal > Man > Tal ≈ Glc in terms of decreasing magnitude of the solvation free-energy. The observed differences are at the limit of the precision reached in the present free-energy calculations and should be taken with some caution. However they are in line with the analysis of solute–solvent hydrogen-bonds, suggesting that Glc is a poorer hydrogen-bond acceptor and Tal a poorer hydrogen-bond donor relative to the solvent (Section 3.6).

The above observations do not support the axial–equatorial hydration model (Section 1), which would suggest a ranking[164,197,201–206] Glc > Gal ≈ Man > Tal in terms of solvation. Neither are they in line with the nonspecific hydration model (Section 1), which predicts a similar ranking[164,167] Glc ≫ Gal > Man ≫ Tal (this ranking is supported experimentally by the analysis of a number of thermodynamic[167,201,370,371] and dynamical[201,203–205,207] solvation parameters), nor are they in line with the specific hydration model (Section 1), which predicts a ranking[210–215] Gal ≫ Glc ≈ Man ≫ Tal (this ranking is supported experimentally by the analysis of other thermodynamic solvation parameters,[198,211,213] of kinetic medium effects on hydrolysis reactions,[210,212] and by measurements of reverse-phase HPLC retension times using pure water as eluent[215]). Note finally that differential affinity to polystyrene matrices and partition coefficients between water and 1-butanol suggests yet a different ranking (Gal > Glc > Man) in terms of decreasing hydrophilicity.[372]

Although there remains considerable uncertainty in the conclusions that should be drawn from the available experimental data about the relative extents of solvation of the four compounds, the reduced hydrophilicity of Tal has been clearly evidenced by (i) deuteration-induced isotope effects on NMR properties;[141] (ii) the particular aggregation properties of Tal-derived amphiphiles;[373] and (iii) the analysis of reverse-phase HPLC experiments using pure water as eluent.[215] In the latter experiments, the retention times of methyl-β-D-galactopyranoside and methyl-β-D-talopyranoside relative to methyl-β-D-glucopyranoside (reference value 1) were found to be 0.78 and 1.11, suggesting a ranking Gal ≫ Glc > Tal in terms of hydrophilicity. This low hydrophilicity of Tal may probably be attributed to the presence of the high-occurrence hydrogen-bond between the 1,3-*syn*-diaxial 2-OH and 4-OH group (Section 3.2) and the resulting reduction of interactions with water (Section 3.6), as already evidenced by previous MD simulations.[214,215] In the specific hydration model, the reduced solvation of Tal is attributed to its good compatibility (i.e., limited disturbance; as compared to Glc, Man and Gal) with the pre-existing hydrogen-bond network of water (camouflage effect[211,212,214–216]), which makes it be recognized as a 'hydrophobic' solute. It should be kept in mind, however, that Tal also differs from the three other hexopyranoses in that it has a more significant furanose component at equilibrium[24] (about 29.1%, as opposed to 0.4%, 0.9% and 6.0% for Glc, Man and Gal), which could also affect the properties monitored experimentally.

In contrast, the equally low hydrophilicity found for Glc in the present simulations appears quite surprising. Although the reason for this behavior is still unclear (namely why Glc forms higher-occurrence intramolecular hydrogen-bonds and is a poorer hydrogen-bond acceptor relative to the solvent, compared to Man and Gal; Section 3.6), it is not impossible that this observation is related to the distinct flexibility of the Glc pyranose ring within the present force field[265] (Section 3.1).

4. Conclusion

The present article reports a comparative study of four β-D-hexopyranoses (Glc, Man, Gal and Tal; Fig. 1) using explicit-solvent (water) molecular dynamics (MD) and vacuum stochastic dynamics (SD) simulations. The main purposes of this study were to (i) provide a detailed and coherent picture of the conformation, dynamics, solvation and relative stabilities of the four hexopyranoses; (ii) investigate the influence of the stereochemistry at two carbon centers (C_2 and C_4) on these properties; (iii) validate the recently developed GROMOS 45A4 carbohydrate force field[265,266] (and provide a solid basis for possible further refinement), by critically comparing simulation results with available experimental and theoretical data on the structural, dynamical, energetic, and solvation properties of the investigated compounds.

The major conclusions of this work can be summarized as follows:

A. In contrast to hexopyranoses in the gas-phase and hexopyranosides (including disaccharides) in solution or in crystals, the dihedral angle ϕ controlling the orientation of the unfunctionalized lactol group in β-hexopyranoses is suggested to preferentially adopt a *t* conformation in aqueous solution, in violation of the *exo*-anomeric effect (g_- preference for β-anomers). This behavior may be related to the comparative weakness of the steric repulsion between the lactol hydrogen and the substituents at C_2 as well as to specific solvation effects. However, although aqueous solvation appears to weaken the *exo*-anomeric effect,[176,333] the observation of such an inversion is to be taken with some caution since the torsional potential used for ϕ in the present force field has been optimized for O_1-methylated compounds[265] rather than reducing hexopyranoses.

B. The formation of intramolecular hydrogen-bonds in aqueous environment appears to be an 'opportunistic' consequence of the close proximity of hydrogen-bonding groups, rather than a major conformational driving force promoting this proximity. In particular, hydrogen-bonding seems to have a very limited influence on the conformational properties of the hydroxymethyl group in water[92,96,101,102,104,131,144,152,157,180,189,190,305,351,354–357] Experimental evidence[121,122,125,126,148,149,155] suggests that this principle also applies to the high-occurrence 1,3-*syn*-diaxial hydrogen-bond between the 2-OH and 4-OH groups in Tal (i.e., this hydrogen-bond occurs because the two groups are 'locked' in l,3-*syn*-diaxial orientation in the most stable $^4C_1$ ring conformer, but does not in itself contribute to the stability of this conformer). In fact, in water, the cumulative effect of steric repulsion and hydrogen-bonding between two 1,3-*syn*-diaxial hydroxyl groups probably represents an overall destabilizing factor for a given molecular conformation.

C. The conformational preferences of the dihedral angle ω controlling the orientation of the hydroxymethyl group in water appear to be dominated by 1,3-*syn*-diaxial repulsion (essentially forbidding the occurrence of g_- when the 4-OH is equatorial, or g_+ when this group is axial), with *gauche* and solvation effects being secondary, and intramolecular hydrogen-bonding essentially negligible.

D. The simulations provide detailed information about the rotational dynamics of the exocyclic hydroxyl groups in water, which is essentially inaccessible to experiment. The present results suggest that these rotations are rapid (10–100 ps timescale) and weakly (but noticeably) correlated, the interconversion between transient hydrogen-bonds of opposite directions involving vicinal or 1,3-*syn*-diaxial hydroxyl groups (flip-flop) following an asynchronous disrotatory pathway. This pathway is probably preferred because it involves (i) minimal dihedral angle changes; (ii) a favorable interaction between the hydroxyl bond dipoles; (iii) a higher orientational freedom for the acceptor group compared to the donor group.

E. The conformational preferences in aqueous environment may be described as a 'weakened' (due to the dielectric screening of intramolecular hydrogen-bonds) form of the vacuum preferences, slightly altered by the presence of specific solvation effects. The latter effects appear in the form of structured solvent environments between the ring and lactol oxygen atoms (contributing to the shift of the ϕ dihedral angle from g_- to *t*), as well as between the 4-OH and hydroxymethyl groups (influencing the relative rotameric populations of this group). These two sites have actually been suggested to represent 'weak spots', where the insertion of a water molecule provides an important cooperativity enhancement to the intramolecular hydrogen-bond network,[162] and may thus correspond to key sites for carbohydrate recognition processes in biochemistry.[361]

F. The calculated epimerization free energies suggest a ranking Glc ≫ Man > Gal ≫ Tal in order of decreasing stability in aqueous solution. Besides an inversion in the relative free energies of Man and Gal, this ranking is identical to that based on three established empirical schemes.[2,18,21,49,67,75] The calculated differences for the C_2 epimerization processes also agree well (arguably better) with direct experimental data. Based on all four estimates, an inversion of the stereochemistry at either C_2 or C_4 from equatorial to axial is associated with a raise in free-energy.

G. The stability differences between the four compounds are dominated by intramolecular effects, while the corresponding differences in solvation free energies are re markably small (at most 1.2 kJ mol^{-1}).

H. The hydrophilicity of a hexopyranose (magnitude of the solvation free-energy) is correlated with the average number of solute–solvent hydrogen-bonds, itself negatively correlated with the average number of intramolecular hydrogen-bonds.

I. The particularly low hydrophilicity of Tal appears related to the formation of a high-occurrence (61%) flip-fop (timescale 1–10 ps; dominantly in the $H_4 \rightarrow O_2$ direction) hydrogen-bonded bridge between the 1,3-*syn*-diaxial 2-OH and 4-OH groups.

Since the early work of Brady,[279,280,293] it is generally accepted that force fields developed for condensed-phase simulations should not be expected to provide a realistic description of sugars in vacuum (e.g., detailed geometries, rotamer populations, vibrational frequencies). However, the results of the present simulations in vacuum appear qualitatively reasonable when compared to available quantum-mechanical and experimental data on hexopyranoses in the gas-phase (counterclockwise hydrogen-bond network, *exo*-anomeric g_- preference for ϕ and hydroxymethyl rotamer preferences for Glc and Man; see below for the discrepancies in the case

of Gal and Tal). Based on this observation, together with points E and G above, it seems unlikely that a force field may perform very well in solution and give completely absurd results in vacuum. For this reason, there is probably still much to learn about force field accuracy and solvation effects (at least in a qualitative sense) from a detailed comparison between simulations in vacuum and in solution.

The GROMOS 45A4 force field[265] used in the present study gives overall reasonable agreement with experimental and quantum-mechanical data (taking into account the large uncertainty often associated with these data in the context of carbohydrates) in terms of conformational preferences (ring conformation, hydroxymethyl rotamer populations), dynamical timescales (hydroxymethyl rotation), and relative stabilities of the four hexopyranoses.

However, the detailed comparison between simulated and experimental results also reveals some deficiencies in this force field: (i) the occurrence of boat conformers (although in very limited amounts) during the simulations, and the specific flexibility of Glc; (ii) the overstabilization of the g_+ rotamer of ω (at the expense of t) in compounds with an axial 4-OH group (Gal, Tal); (iii) a possible overstabilization of the t rotamer of ϕ (at the expense of g_-; point A above); and (iv) a possibly incorrect description of Glc intramolecular hydrogen-bonding and hydration (unexpectedly low hydrophilicity). Further refinement of the force field so as to remedy these deficiencies is currently in progress.

Acknowledgements

Financial support from the Swiss National Foundation, Grant No. 21-105397, is gratefully acknowledged. Many thanks to Zrinka Gattin for numerous discussions and her help in the literature search.

Supplementary data

Supplementary data associated with this article can be found, in the online version, at doi:10.1016/j.carres.2007.05.011.

References

1. Lehmann, J. *Carbohydrates Structure and Biology*; Georg Thieme: Stuttgart, Germany, 1998.
2. Rao, V. S. R.; Qasba, P. K.; Balaji, P. V.; Chandrasekaran, R. *Conformation of Carbohydrates*; Harwood Academic: Amsterdam, The Netherlands, 1998.
3. Dwek, R. A.; Edge, C. J.; Harvey, D. J.; Wormald, M. R. *Annu. Rev. Biochem.* **1993**, *62*, 65–100.
4. Rice, K. G.; Wu, P.; Brand, L.; Lee, Y. C. *Curr. Opin. Struct. Biol.* **1993**, *3*, 669–674.
5. Dwek, R. A. *Chem. Rev.* **1996**, *96*, 683–720.
6. Davis, A. P.; Wareham, R. S. *Angew. Chem., Int. Ed.* **1999**, *38*, 2978–2996.
7. Rüdiger, H.; Siebert, H.-C.; Solís, D.; Jiménez-Barbero, J.; Romero, A.; von der Lieth, C.-W.; Diaz-Mauriño, T.; Gabius, H.-J. *Curr. Med. Chem.* **2000**, *7*, 389–416.
8. Wormald, M. R.; Petrescu, A. J.; Pao, Y.-L.; Glithero, A.; Elliott, T. *Chem. Rev.* **2002**, *102*, 371–386.
9. Lowe, J. B.; Marth, J. D. *Annu. Rev. Biochem.* **2003**, *72*, 643–691.
10. Tunnacliffe, A.; Lapinski, J. *Philos. Trans. R. Soc. London Ser. B* **2003**, *358*, 1755–1771.
11. Gabius, H.-J.; André, S.; Kaltner, H.; Siebert, H.-C. *Biochim. Biophys. Acta* **2002**, *1572*, 165–177.
12. Hricovini, M. *Curr. Med. Chem.* **2004**, *11*, 2565–2583.
13. Gabius, H.-J.; Siebert, H.-C.; André, S.; Jiménez-Barbero, J.; Rüdiger, H. *ChemBioChem* **2004**, *5*, 740–764.
14. Crowe, J. H.; Crowe, L. M.; Wolkers, W. F.; Oliver, A. E.; Ma, X.; Auh, J.-H.; Tang, M.; Zhu, S.; Norris, J.; Tablin, F. *Integr. Comp. Biol.* **2005**, *45*, 810–820.
15. Jiménez-Barbero, J.; Asensio, J. L.; Cuevas, G.; Canales, A.; Fernández-Alonso, M. C.; Cañada, F. J. *Biocatal. Biotransform.* **2006**, *24*, 13–22.
16. Ramesh, H. P.; Tharanathan, R. N. *Grit. Rev. Biotech.* **2003**, *23*, 149–173.
17. Pigman, W.; Isbell, H. S. *Adv. Carbohydr. Chem. Biochem.* **1968**, *23*, 11–57.
18. Angyal, S. J. *Angew. Chem., Int. Ed. Engl.* **1969**, *8*, 157–166.
19. Angyal, S. J.; Pickles, V. A. *Aust. J. Chem.* **1972**, *25*, 1695–1710.
20. Bentley, R. *Annu. Rev. Biochem.* **1972**, *41*, 953–996.
21. Angyal, S. J. *Adv. Carbohydr. Chem. Biochem.* **1984**, *42*, 15–69.
22. Angyal, S. J. *Adv. Carbohydr. Chem. Biochem.* **1991**, *42*, 19–35.
23. Ma, B.; Schaefer, H. F., III; Allinger, N. L. *J. Am. Chem. Soc.* **1998**, *120*, 3411–3422.
24. Zhu, Y.; Zajicek, J.; Serianni, A. S. *J. Org. Chem.* **2001**, *66*, 6244–6251.
25. Lewis, B. E.; Choytun, N.; Schramm, V. L.; Bennet, A. J. *J. Am. Chem. Soc.* **2006**, *128*, 5049–5058.
26. Danilova, V. A.; Krivdin, L. B. *Russ. J. Org. Chem.* **2004**, *40*, 57–62.
27. DeMatteo, M. P.; Snyder, N. L.; Morton, M.; Baldisseri, D. M.; Hadad, C. M.; Peczuh, M. W. *J. Org. Chem.* **2004**, *70*, 24–38.
28. Pakulski, Z. *Polish J. Chem.* **2006**, *80*, 1293–1326.
29. Grindley, T. B.; Gulasekharam, V. *J. Chem. Soc., Chem. Commun.* **1978**, *23*, 1073–1074.
30. Snyder, J. R.; Serianni, A. S. *J. Org. Chem.* **1986**, *51*, 2694–2702.
31. Lee, C. Y.; Acree, T. E.; Schallenberger, R. S. *Carbohydr. Res.* **1969**, *9*, 356–360.
32. Acree, T. E.; Schallenberger, R. S.; Lee, Y.; Einset, J. W. *Carbohydr. Res.* **1969**, *10*, 355–360.
33. Wertz, P. W.; Carver, J. C.; Anderson, L. *J. Am. Chem. Soc.* **1981**, *103*, 3916–3922.
34. Serianni, A. S.; Pierce, J.; Huang, S.-G.; Barker, R. *J. Am. Chem. Soc.* **1982**, *104*, 4037–4044.
35. Snyder, J. R.; Johnston, E. R.; Serianni, A. S. *J. Am. Chem. Soc.* **1989**, *111*, 2681–2687.
36. Behrends, R.; Kaatze, U. *Chem. Phys. Chem.* **2005**, *6*, 1133–1145.
37. Bubb, W. A. *Concepts Magn. Reson. A* **2003**, *19*, 1–19.

38. Reeves, R. E. *Adv. Carbohydr. Chem.* **1951**, *6*, 107–134.
39. Angyal, S. J.; Klavins, J. E.; Mills, J. A. *Aust. J. Chem.* **1974**, *27*, 1075–1086.
40. Hayward, L. D.; Angyal, S. J. *Carbohydr. Res.* **1977**, *53*, 13–20.
41. Reeves, R. E. *J. Am. Chem. Soc.* **1950**, *72*, 1499–1506.
42. Jensen, F. R.; Bushweller, C. H. *Adv. Alicycl. Chem.* **1971**, *3*, 139–194.
43. Mäler, L.; Widmalm, G.; Kowalewski, J. *J. Phys. Chem.* **1996**, *100*, 17103–17110.
44. Kleinpeter, E. *Adv. Heterocycl. Chem.* **2004**, *86*, 41–127.
45. Pickett, H. M.; Strauss, H. L. *J. Am. Chem. Soc.* **1970**, *92*, 7281–7290.
46. Cremer, D.; Pople, J. A. *J. Am. Chem. Soc.* **1975**, *97*, 1354–1358.
47. French, A. D.; Brady, J. W. *ACS Symp. Ser.* **1990**, *430*, 1–19.
48. Forster, M. J.; Mulloy, B. *Biopolymers* **1993**, *33*, 575–588.
49. Dowd, M. K.; French, A. D.; Reilly, P. J. *Carbohydr. Res.* **1994**, *264*, 1–19.
50. Dowd, M. K.; French, A. D.; Reilly, P. J. *Aust. J. Chem.* **1996**, *49*, 327–335.
51. Ernst, S.; Venkataraman, G.; Sasisekharan, V.; Langer, R.; Cooney, C. L.; Sasisekharan, R. *J. Am. Chem. Soc.* **1998**, *120*, 2099–2107.
52. Dowd, M. K.; Rockey, W. M.; French, A. D.; Reilly, P. J. *J. Carbohydr. Chem.* **2002**, *21*, 11–25.
53. Navarro, D.; Stortz, C. A. *Carbohydr. Res.* **2005**, *340*, 2030–2038.
54. Sanderson, P. N.; Huckerby, T. N.; Nieduszynski, I. A. *Glycoconjugate J.* **1985**, *2*, 109–120.
55. Cano, F. H.; Foces-Foces, C.; Jimenez-Barbero, J.; Bernabe, M.; Martin-Lomas, M. *Carbohydr. Res.* **1987**, *145*, 319–327.
56. Ragazzi, M.; Ferro, D. R.; Provasoli, A. *J. Comput. Chem.* **1986**, *7*, 105–112.
57. Ferro, D. R.; Provasoli, A.; Ragazzi, M.; Torri, G.; Casu, B.; Gatti, G.; Jacquinet, J.-C.; Sinay, P.; Petitou, M.; Choay, J. *J. Am. Chem. Soc.* **1986**, *108*, 6773–6778.
58. Sanderson, P. N.; Huckerby, T. N.; Nieduszynski, I. A. *Biochem. J.* **1987**, *243*, 175–181.
59. Giuliano, R. M.; Bryan, R. F.; Hartley, P.; Peckler, S.; Woode, M. K. *Carbohydr. Res.* **1989**, *191*, 1–11.
60. Ferro, D. R.; Provasoli, A.; Ragazzi, M.; Casu, B.; Torri, G.; Bossenec, V.; Perly, B.; Sinay, P.; Petitou, M.; Choay, J. *Carbohydr. Res.* **1990**, *195*, 157–167.
61. Horita, D. A.; Hadjuk, P. J.; Lerner, L. E. *Glycoconjugate J.* **1997**, *14*, 691–696.
62. Coxon, B.; Reynolds, R. C. *Carbohydr. Res.* **2001**, *331*, 461–467.
63. Uccello-Barretta, G.; Sicoli, G.; Balzano, F.; Salvadori, P. *Carbohydr. Res.* **2003**, *338*, 1103–1107.
64. Roslund, M. U.; Klika, K. D.; Lehtilä, R. L.; Tähtinen, P.; Silanpää, R.; Leino, R. *J. Org. Chem.* **2004**, *69*, 18–25.
65. Hakkarainen, B.; Fujita, K.; Inirnel, S.; Kenne, L.; Sandström, C. *Carbohydr. Res.* **2005**, *340*, 1539–1545.
66. Hassel, O.; Ottar, B. *Acta Chem. Scand.* **1947**, *1*, 929–943.
67. Angyal, S. J. *Aust. J. Chem.* **1968**, *21*, 2737–2746.
68. Corey, E. J.; Feiner, N. F. *J. Org. Chem.* **1980**, *45*, 757–764.
69. Corey, E. J.; Feiner, N. F. *J. Org. Chem.* **1980**, *45*, 765–780.
70. Reeves, R. E. *J. Am. Chem. Soc.* **1954**, *76*, 4595–4598.
71. Angyal, S. J.; McHugh, D. J. *Chem. Ind.* **1956**, *41*, 1147–1148.
72. Angyal, S. J.; Pickles, V. A.; Ahluwahlia, R. *Carbohydr. Res.* **1966**, *1*, 365–370.
73. Sundararajan, P. R.; Rao, V. S. R. *Tetrahedron* **1968**, *24*, 289–295.
74. Rao, V. S. R.; Vijayalakshmi, K. S.; Sundararajan, P. R. *Carbohydr. Res.* **1971**, *17*, 341–352.
75. Vijayalakshmi, K. S.; Rao, V. S. R. *Carbohydr. Res.* **1972**, *22*, 413–424.
76. Vijayalakshmi, K. S.; Yathindra, N.; Rao, V. S. R. *Carbohydr. Res.* **1973**, *31*, 173–181.
77. Joshi, N. V.; Rao, V. S. R. *Biopolymers* **1979**, *18*, 2993–3004.
78. Zhdanov, Y. A.; Malysheva, E. N. *Carbohydr. Res.* **1972**, *24*, 87–93.
79. Barrows, S. E.; Dulles, F. J.; Cramer, C. J.; French, A. D.; Truhlar, D. G. *Carbohydr. Res.* **1995**, *276*, 219–251.
80. Csonka, G. I.; Éliás, K.; Csizmadia, I. G. *Chem. Phys. Lett.* **1996**, *257*, 49–60.
81. Appell, M.; Strati, G.; Willett, J. L. *Carbohydr. Res.* **2004**, *339*, 537–551.
82. Franks, F.; Lillford, P. J.; Robinson, G. *J. Chem. Soc., Faraday Trans. I* **1989**, *85*, 2417–2426.
83. Augé, J.; David, S. *Tetrahedron* **1984**, *40*, 2101–2106.
84. Reuben, J. *J. Am. Chem. Soc.* **1985**, *107*, 5867–5870.
85. Kurihara, Y.; Ueda, K. *Carbohydr. Res.* **2006**, *341*, 2565–2574.
86. Polacek, R.; Stenger, J.; Kaatze, U. *J. Chem. Phys.* **2002**, *116*, 2973–2982.
87. Stenger, J.; Cowman, M. K.; Eggers, F.; Eyring, E. M.; Kaatze, U.; Petrucci, S. *J. Phys. Chem. B* **2000**, *104*, 4782–4790.
88. Hagen, R.; Kaatze, U. *J. Chem. Phys.* **2004**, *120*, 9656–9664.
89. Hajduk, P. J.; Horita, D. A.; Lerner, L. E. *J. Am. Chem. Soc.* **1993**, *115*, 9196–9201.
90. Haasnoot, C. A. G.; De Leeuw, F. A. A. M.; Altona, C. *Tetrahedron* **1980**, *36*, 2783–2792.
91. Tvaroška, I.; Hricovíni, M.; Petráková, E. *Carbohydr. Res.* **1989**, *189*, 359–362.
92. Bock, K.; Duus, J. O. *J. Carbohydr. Chem.* **1994**, *13*, 513–543.
93. Tvaroška, I.; Gajdoš, J. *Carbohydr. Res.* **1995**, *271*, 151–162.
94. Bose, B.; Zhao, S.; Stenutz, R.; Cloran, F.; Bondo, P. B.; Bondo, G.; Hertz, B.; Carmichael, I.; Serianni, A. S. *J. Am. Chem. Soc.* **1998**, *120*, 11158–11173.
95. Stenutz, R.; Carmichael, I.; Widmalm, G.; Serianni, A. S. *J. Org. Chem.* **2002**, *67*, 949–958.
96. Thibaudeau, C.; Stenutz, R.; Hertz, B.; Klepach, T.; Zhao, S.; Wu, Q.; Carmichael, I.; Serianni, A. S. *J. Am. Chem. Soc.* **2004**, *126*, 15668–15685.
97. Kraszni, M.; Szakács, Z.; Noszál, B. *Anal. Bioanal. Chem.* **2004**, *378*, 1149–1163.
98. Suzuki, T.; Kawashima, H.; Sota, T. *J. Phys. Chem. B* **2006**, *110*, 2405–2418.
99. Nishida, Y.; Ohrui, H.; Meguro, H. *Tetrahedron Lett.* **1984**, *25*, 1575–1578.
100. Nishida, Y.; Hori, H.; Ohrui, H.; Meguro, H. *J. Carbohydr. Chem.* **1988**, *7*, 239–250.
101. Abraham, R. J.; Chambers, E. J.; Thomas, W. A. *Magn. Reson. Chem.* **1992**, *30*, S60–S65.
102. Abraham, R. J.; Chambers, E. J.; Thomas, W. A. *Magn. Reson. Chem.* **1994**, *32*, 248–254.
103. Brochier-Salon, M.-C.; Morin, C. *Magn. Reson. Chem.* **2000**, *38*, 1041–1042.
104. Tvaroška, I.; Taravel, F. R.; Utille, J. P.; Carver, J. P. *Carbohydr. Res.* **2002**, *337*, 353–367.

105. Hori, H.; Nishida, Y.; Ohrui, H.; Meguro, H. *J. Carbohydr. Chem.* **1990**, *9*, 601–618.
106. Behrends, R.; Cowman, M. K.; Eggers, F.; Eyring, E. M.; Kaatze, U.; Majewski, J.; Petrucci, S.; Richmann, K.-H.; Riech, M. *J. Am. Chem. Soc.* **1997**, *119*, 2182–2186.
107. Poppe, L. *J. Am. Chem. Soc.* **1993**, *115*, 8241–8426.
108. Dais, P.; Marcheussault, R. H. *Macromolecules* **1991**, *24*, 4611–4614.
109. Duus, J. O.; Gotfredsen, C. H.; Bock, K. *Chem. Rev.* **2000**, *100*, 4589–4614.
110. Hawley, J.; Bampos, N.; Aboitiz, N.; Jiménez-Barbero, J.; López de la Paz, M.; Sanders, J. K. M.; Carmona, P.; Vicent, C. *Eur. J. Org. Chem.* **2002**, *12*, 1925–1936.
111. Fabri, D.; Williams, M. A. K.; Halstead, T. K. *Carbohydr. Res.* **2005**, *340*, 889–905.
112. Sandström, C.; Kenne, L. *ACS Symp. Ser.* **2006**, *930*, 114–132.
113. Zhbankov, R. G. *J. Mol. Struct.* **1992**, *270*, 523–539.
114. Carmona, P.; Molina, M.; Aboitiz, N.; Vicent, C. *Biopolymers* **2002**, *67*, 20–25.
115. López de la Paz, M.; Ellis, G.; Pérez, M.; Perkins, J.; Jiménez-Barbero, J.; Vicent, C. *Eur. J. Org. Chem.* **2002**, *5*, 840–855.
116. Eliel, E. L.; Lukach, C. A. *J. Am. Chem. Soc.* **1957**, *79*, 5986–5992.
117. Kabayama, M. A.; Patterson, D. *Can. J. Chem.* **1958**, *36*, 563–573.
118. Franzus, B.; Hudson, B. E., Jr. *J. Org. Chem.* **1963**, *28*, 2238–2244.
119. Subbotin, O. A.; Sergeyev, N. M. *Anal. Chem.* **1976**, *48*, 545–546.
120. Eliel, E. L.; Hargrave, K. D.; Petrusiewicz, K. M.; Manoharan, M. *J. Am. Chem. Soc.* **1982**, *104*, 3635–3643.
121. Bacon, J. F.; van der Maas, J. H.; Dixon, J. R.; George, W. O.; Mclntyre, P. S. *Spectrochim. Acta, Part A* **1989**, *45*, 1313–1318.
122. Abraham, R. J.; Chambers, E. J.; Thomas, W. A. *J. Chem. Soc. Perkin Trans. 2* **1993**, 1061–1066.
123. Boiadjiev, S. E.; Lightner, D. A. *J. Am. Chem. Soc.* **2000**, *122*, 11328–11339.
124. Lewis, B. R.; Schramm, V. L. *J. Am. Chem. Soc.* **2001**, *123*, 1327–1336.
125. de Oliveira, P. R.; Rittner, R. *Spectrochim. Acta, Part A* **2005**, *62*, 30–37.
126. de Oliveira, P. R.; Rittner, R. *J. Mol. Struct.* **2005**, *743*, 69–72.
127. Weldon, A. J.; Vickrey, T. L.; Tschumper, G. S. *J. Phys. Chem. A* **2005**, *109*, 11073–11079.
128. Lii, J.-H.; Chen, K.-H.; Grindley, T. B.; Allinger, N. L. *J. Comput. Chem.* **2003**, *24*, 1490–1503.
129. Lii, J.-H.; Chen, K.-H.; Allinger, N. L. *J. Comput. Chem.* **2003**, *24*, 1504–1513.
130. Jefrey, G. A. *Acta Crystallogr., Sect. B* **1990**, *46*, 89–103.
131. Abraham, R. J.; Chambers, E. J.; Thomas, W. A. *Carbohydr. Res. C* **1992**, *226*, 1–5.
132. Alabugin, I. V. *J. Org. Chem.* **2000**, *65*, 3910–3919.
133. Cortés-Guzmán, F.; Hernández-Trujillo, J.; Cuevas, G. *J. Phys. Chem. A* **2003**, *107*, 9253–9256.
134. Taddei, F.; Kleinpeter, E. *J. Mol. Struct.* **2004**, *683*, 29–41.
135. Kleinpeter, E.; Rolla, N.; Koch, A.; Taddei, F. *J. Org. Chem.* **2006**, *71*, 4393–4399.
136. Jensen, F. R.; Bushweller, C. H.; Beck, B. H. *J. Am. Chem. Soc.* **1969**, *91*, 344–351.
137. Wilberg, K. B.; Hammer, J. D.; Castejon, H.; Bailey, W. F.; DeLeon, E. L.; Jarret, R. M. *J. Org. Chem.* **1999**, *64*, 2085–2095.
138. Harvey, J. M.; Symons, M. C. R.; Naftalin, R. J. *Nature* **1976**, *261*, 435–436.
139. Harvey, J. M.; Symons, M. C. R. *J. Solution Chem.* **1978**, *7*, 571–586.
140. Pfeffer, P. E.; Valentine, K. M.; Parrish, F. W. *J. Am. Chem. Soc.* **1979**, *101*, 1265–1274.
141. Reuben, J. *J. Am. Chem. Soc.* **1984**, *106*, 6180–6186.
142. Dais, P.; Perlin, A. S. *Carbohydr. Res.* **1987**, *169*, 159–169.
143. Adams, B.; Lerner, L. *J. Am. Chem. Soc.* **1992**, *114*, 4827–4829.
144. Beeson, C.; Pham, N.; Shipps, G., Jr.; Dix, T. A. *J. Am. Chem. Soc.* **1993**, *115*, 6803–6812.
145. Bolvig, S.; Hansen, P. E. *Curr. Org. Chem.* **2000**, *4*, 19–54.
146. Bernet, B.; Vasella, A. *Helv. Chim. Acta* **2000**, *83*, 995–1021.
147. Bosco, M.; Picotti, F.; Radoicovich, A.; Rizzo, R. *Biopolymers* **2000**, *53*, 272–280.
148. Abraham, R. J.; Byrne, J. J.; Griffiths, L.; Koniotou, R. *Magn. Reson. Chem.* **2005**, *43*, 611–624.
149. de Oliveira, P. R.; Rittner, R. *Spectrochim. Acta, Part A* **2005**, *61*, 1737–1745.
150. Kuhn, L. P. *J. Am. Chem. Soc.* **1962**, *74*, 2492–2499.
151. Casu, B.; Reggiani, M.; Gallo, G. G.; Vigevani, A. *Tetrahedron* **1966**, *22*, 3061–3083.
152. Lemieux, R. U.; Brewer, J. T. *Adv. Chem.* **1973**, *117*, 121–146.
153. Durier, V.; Tristram, F.; Vergoten, G. *Carbohydr. Res.* **1997**, *395*, 81–90.
154. Simperler, A.; Watt, S. W.; Bonnet, P. A.; Jones, W.; Motherwell, W. D. S. *Cryst. Eng. Commun.* **2006**, *8*, 589–600.
155. Tominaga, T.; Tenma, S.; Watanabe, H. *J. Chem. Soc., Faraday Trans* **1996**, *92*, 1863–1867.
156. Luque, F. J.; López, J. M.; López de la Paz, M.; Vicent, C.; Orozco, M. *J. Phys. Chem. A* **1998**, *102*, 6690–6696.
157. Roën, A.; Padrón, J. I.; Vásquez, J. T. *J. Org. Chem.* **2002**, *68*, 4615–4630.
158. Tse, Y.-C.; Newton, M. D. *J. Am. Chem. Soc.* **1977**, *99*, 611–613.
159. Jeffrey, G. A.; Lewis, L. *Carbohydr. Res.* **1978**, *60*, 178–182.
160. Jeffrey, G. A.; Mitra, J. *Acta Crystallogr., Sect. B* **1983**, *39*, 469–480.
161. Engelsen, S. B.; Hervé du Penhoat, C.; Pérez, S. *J. Phys. Chem.* **1995**, *99*, 13334–13350.
162. Carcabal, P.; Jockusch, R. A.; Hünig, I.; Snoek, L. C.; Kroemer, R. T.; Davis, B. G.; Gamblin, D. P.; Compagnin, I.; Oomens, J.; Simons, J. P. *J. Am. Chem. Soc.* **2005**, *127*, 11414–11425.
163. Simons, J. P.; Jockusch, R. A.; Carcabal, P.; Hünig, I.; Kroemer, R. T.; McLeod, N. A.; Snoek, L. C. *Int. Rev. Phys. Chem.* **2005**, *24*, 489–531.
164. Dashnau, J. L.; Sharp, K. A.; Vanderkooi, J. M. *J. Phys. Chem. B* **2005**, *109*, 24152–24159.
165. Petillo, P. A.; Lerner, L. A. *ACS Symp. Ser.* **1993**, *539*, 156–175.
166. Praly, J.-P.; Lemieux, R. U. *Can. J. Chem.* **1987**, *65*, 213–223.
167. Walkinshaw, M. D. *J. Chem. Soc., Perkin Trans. 2* **1987**, 1903–1906.
168. Edward, J. T. *Chem. Ind.* **1955**, *36*, 1102–1104.

169. Pierson, G. O.; Runquist, O. *J. Org. Chem.* **1968**, *33*, 2572–2574.
170. de Hoog, A. J.; Buys, H. R.; Altona, C.; Havinga, E. *Tetrahedron* **1969**, *25*, 3365–3375.
171. Lemieux, R. U.; Koto, S. *Tetrahedron* **1974**, *30*, 1933–1944.
172. Inagaki, S.; Iwase, K.; Mori, Y. *Chem. Lett.* **1986**, *3*, 417–420.
173. Juaristi, E.; Cuevas, G. *Tetrahedron* **1992**, *48*, 5019–5087.
174. Salzner, U.; von Ragué Schleyer, P. *J. Org. Chem.* **1994**, *59*, 2138–2155.
175. Graczyk, P. P.; Mikolajczyk, M. *Top. Stereochem.* **1994**, *21*, 159–349.
176. Tvaroška, I.; Carver, J. P. *Carbohydr. Res.* **1998**, *309*, 1–9.
177. Lii, J.-H.; Chen, K.-H.; Durkin, K.; Allinger, N. L. *J. Comput. Chem.* **2003**, *24*, 1473–1489.
178. Pérez, S.; Marchessault, R. H. *Carbohydr. Res.* **1978**, *65*, 114–120.
179. Thogersen, H.; Lemieux, R. U.; Bock, K.; Meyer, B. *Can. J. Chem.* **1982**, *60*, 44–57.
180. Mayato, C.; Dorta, R. L.; Vázquez, J. T. *Tetrahedron: Asymmetry* **2004**, *15*, 2385–2397.
181. Wolfe, S. *Acc. Chem. Res.* **1970**, *5*, 102–111.
182. Wolfe, S.; Tel, L. M.; Haines, W. J.; Robb, M. A.; Csizmadia, I. G. *J. Am. Chem. Soc.* **1973**, *95*, 4863–4870.
183. Epiotis, N. D.; Sarkanen, S.; Bjorkquist, D.; Bjorkquist, L.; Yates, R. *J. Am. Chem. Soc.* **1974**, *96*, 4075–4084.
184. Zefirov, N. S.; Gurvich, L. G.; Shashkov, A. S.; Krimer, M. Z.; Vorobeva, E. A. *Tetrahedron* **1976**, *32*, 1211–1219.
185. Abe, A.; Mark, J. E. *J. Am. Chem. Soc.* **1976**, *98*, 6468–6476.
186. Zefirov, N. S.; Samoshin, V. V.; Subbotin, O. A.; Baranekov, V. I. *Tetrahedron* **1978**, *34*, 2953–2959.
187. Abe, A.; Inomata, K. *J. Mol. Struct.* **1991**, *245*, 399–402.
188. Juaristi, E.; Antúnez, S. *Tetrahedron* **1992**, *48*, 5941–5950.
189. de Vries, N. K.; Buck, H. M. *Carbohydr. Res.* **1987**, *165*, 1–16.
190. de Vries, N. K.; Buck, H. M. *Recl. Trav. Chim. Pays-Bas* **1987**, *106*, 453–460.
191. Alabugin, I. V.; Manoharan, M.; Zeidan, T. A. *J. Am. Chem. Soc.* **2003**, *125*, 14014–14031.
192. Franks, F. *Cryobiology* **1983**, *20*, 335–345.
193. Franks, F. *Pure Appl. Chem.* **1987**, *59*, 1189–1202.
194. Onodera, K.; Hirano, S.; Masuda, F. *Carbohydr. Res.* **1968**, *7*, 27–37.
195. Liu, Q.; Brady, J. W. *J. Am. Chem. Soc.* **1996**, *118*, 12276–12286.
196. Costa, F. S.; Eusébio, M. E.; Redinha, J. S.; Leitao, M. L. P. *J. Chem. Thermodyn.* **2000**, *32*, 311–317.
197. Bonnet, A.; Chisholm, J.; Motherwell, W. D. S.; Jones, W. *Cryst. Eng. Commun.* **2005**, *7*, 71–75.
198. Chalikian, T. V. *J. Phys. Chem. B* **1998**, *102*, 6921–6926.
199. Engelsen, S. B.; Monteiro, C.; Hervé de Penhoat, C.; Pérez, S. *Biophys. Chem.* **2001**, *93*, 103–127.
200. Almond, A. *Carbohydr. Res.* **2005**, *340*, 907–920.
201. Uedaira, H.; Uedaira, H. *J. Solution Chem.* **1985**, *14*, 27–34.
202. Uedaira, H.; Uedaira, H. *J. Chem. Thermodyn.* **1985**, *17*, 901–902.
203. Uedaira, H.; Ishimura, M. *Bull. Chem. Soc. Jpn.* **1989**, *62*, 574–575.
204. Uedaira, H.; Ikura, M.; Uedaira, H. *Bull. Chem. Soc. Jpn.* **1989**, *62*, 1–4.
205. Uedaira, H.; Ishimura, M.; Tsuda, S.; Uedaira, H. *Bull. Chem. Soc. Jpn.* **1990**, *63*, 3376–3379.
206. Uedaira, H.; Uedaira, H. *Cell. Mol. Biol.* **2001**, *47*, 823–829.
207. Tait, M. J.; Suggett, A.; Franks, F.; Ablett, S.; Quickenden, P. A. *J. Solution Chem.* **1972**, *1*, 131–151.
208. Franks, F.; Reid, D. S.; Suggett, A. *J. Solution Chem.* **1973**, *2*, 99–118.
209. Suggett, A. *J. Solution Chem.* **1976**, *5*, 33–46.
210. Galema, S. A.; Hoiland, H. *J. Am. Chem. Soc.* **1990**, *112*, 9665–9666.
211. Galema, S. A.; Hoiland, H. *J. Phys. Chem.* **1991**, *95*, 5321–5326.
212. Galema, S. A.; Blandamer, M. J.; Engberts, J. B. F. N. *J. Org. Chem.* **1992**, *57*, 1995–2001.
213. Galema, S. A.; Engberts, J. B. F. N.; Hoiland, H.; Forland, G. M. *J. Phys. Chem.* **1993**, *97*, 6885–6889.
214. Galema, S. A.; Howard, E.; Engberts, J. B. F. N.; Grigera, J. R. *Carbohydr. Res.* **1994**, *265*, 215–225.
215. Cheetham, N. W. H.; Lam, K. *Carbohydr. Res.* **1996**, *282*, 13–23.
216. Cheetham, N. W. H.; Dasgupta, P. *Aust. J. Chem.* **2005**, *58*, 803–809.
217. Woods, R. J. *Curr. Opin. Struct. Biol.* **1995**, *5*, 591–598.
218. Imberty, A. *Curr. Opin. Struct. Biol.* **1997**, *7*, 617–623.
219. Woods, R. J. *Glycoconjugate J.* **1998**, *15*, 209–216.
220. Madsen, L. J.; Ha, S. N.; Tran, V. H.; Brady, J. W. *ACS Symp. Ser.* **1990**, *430*, 69–90.
221. Imberty, A.; Pérez, S. *Curr. Opin. Struct. Biol.* **2000**, *7*, 617–623.
222. Pérez, S.; Mulloy, B. *Curr. Opin. Struct. Biol.* **2005**, *15*, 517–524.
223. Laederach, A.; Reilly, P. J. *Proteins: Struct. Fund. Bioinf.* **2005**, *60*, 591–597.
224. Dyekjaer, J. D.; Woods, R. J. *ACS Symp. Ser.* **2006**, *930*, 203–219.
225. Queyroy, S.; Neyertz, S.; Brown, D.; Müller-Plathe, F. *Macromolecules* **2004**, *37*, 7338–7350.
226. Limbach, H. J.; Kremer, K. *Trends Food Sci. Technol.* **2006**, *17*, 215–219.
227. Allinger, N. L. *J. Am. Chem. Soc.* **1977**, *25*, 8127–8134.
228. Allinger, N. L. *J. Am. Chem. Soc.* **1989**, *111*, 8551–8566.
229. Allinger, N. L. *J. Am. Chem. Soc.* **1989**, *111*, 8566–8575.
230. Allinger, N. L. *J. Am. Chem. Soc.* **1989**, *111*, 8576–8582.
231. Allinger, N. L.; Chen, K.-H.; Lii, J.-H. *J. Comput. Chem.* **2003**, *24*, 1447–1472.
232. Rasmussen, K. *J. Mol. Struct.* **1997**, *395*, 91–106.
233. Hwang, M.-J.; Ni, X.; Waldman, M.; Ewig, C. S.; Hagler, A. T. *Biopolymers* **1998**, *45*, 435–468.
234. Momany, F. A.; Rone, R. *J. Comput. Chem.* **1992**, *13*, 888–900.
235. Grootenhuis, P. D. J.; Haasnoot, C. A. G. *Mol. Simulat.* **1993**, *10*, 75–95.
236. Kouwijzer, M. L. C. E.; Grootenhuis, P. D. J. *J. Phys. Chem.* **1995**, *99*, 13426–13436.
237. Senderowitz, H.; Parish, C.; Still, W. C. *J. Am. Chem. Soc.* **1996**, *118*, 2078–2086.
238. Senderowitz, H.; Still, W. C. *J. Org. Chem.* **1997**, *62*, 1427–1438.
239. Ha, S. N.; Giammona, A.; Field, M.; Brady, J. W. *Carbohydr. Res.* **1988**, *180*, 207–221.
240. Palma, R.; Zuccato, P.; Himmel, M. E.; Liang, G.; Brady, J. W. Molecular mechanics studies of cellulases. In *Glycosyl Hydrolases in Biomass Conversions*; Himmel, M. E., Ed.; American Chemical Society: Washington DC, USA, 2000; pp 112–130.
241. Kuttel, M.; Brady, J. W.; Naidoo, K. J. *J. Comput. Chem.* **2002**, *23*, 1236–1243.

242. Reiling, S.; Schlenkrich, M.; Brickmann, J. *J. Comput. Chem.* **1995**, *17*, 450–568.
243. Eklund, R.; Widmalm, G. *Carbohydr. Res.* **2003**, *338*, 393–398.
244. Homans, S. W. *Biochemistry* **1990**, *29*, 9110–9118.
245. Glennon, T. M.; Zheng, Y.-J.; Le Grand, S. M.; Schutzberg, B. A.; Merz, K. M., Jr. *J. Comput. Chem.* **1994**, *15*, 1019–1040.
246. Glennon, T. M.; Merz, K. M., Jr. *J. Mol. Struct.* **1997**, *395*, 157–171.
247. Gregurick, S. K.; Liu, J. H.-Y.; Brant, D. A.; Gerber, R. G. *J. Phys. Chem. B* **1999**, *103*, 3476–3488.
248. Woods, R. J.; Dwek, R. A.; Edge, C. J.; Fraser-Reid, B. *J. Phys. Chem.* **1995**, *99*, 3832–3846.
249. Woods, R. J.; Chappelle, R. *J. Mol. Struct.* **2000**, *527*, 149–156.
250. Basma, M.; Sundara, S.; Calgan, D.; Vernali, T.; Woods, R. J. *J. Comput. Chem.* **2001**, *22*, 1125–1137.
251. Kirschner, K. N.; Woods, R. J. *Proc. Natl. Acad. Sci. U.S.A.* **2001**, *98*, 10541–10545.
252. Momany, F. A.; Willett, J. L. *Carbohydr. Res.* **2000**, *326*, 194–209.
253. Momany, F. A.; Willett, J. L. *Carbohydr. Res.* **2000**, *326*, 210–226.
254. Simmerling, C.; Fox, T.; Kollman, P. A. *J. Am. Chem. Soc.* **1998**, *120*, 5771–5782.
255. Damm, W.; Frontera, A.; Tirado-Rives, J.; Jorgensen, W. *J. Comput. Chem.* **1997**, *18*, 1955–1970.
256. Kony, D.; Damm, W.; Stoll, S.; van Gunsteren, W. F. *J. Comput. Chem.* **2002**, *23*, 1416–1429.
257. Kony, D.; Damm, W.; Stoll, S.; Hünenberger, P. H. *J. Phys. Chem. B* **2004**, *108*, 5815–5826.
258. van Gunsteren, W. F.; Billeter, S. R.; Eising, A. A.; Hünenberger, P. H.; Krüger, P.; Mark, A. E.; Scott, W. R. P.; Tironi, I. G. *The GRO-MOS96 Manual and User Guide*; Verlag der Fachvereine: Zürich, 1996.
259. Scott, W. R. P.; Hünenberger, P. H.; Tironi, I. G.; Mark, A. E.; Billeter, S. R.; Fennen, J.; Torda, A. E.; Huber, T.; Krüger, P.; van Gunsteren, W. F. *J. Phys. Chem. A* **1999**, *103*, 3596–3607.
260. Kouwijzer, M. L. C. E.; van Eijck, B. P.; Kooijman, H.; Kroon, J. *Acta Crystallogr., Sect. B* **1995**, *51*, 209–220.
261. Klewinghaus, P.; van Eijck, B. P.; Kouwijzer, M. L. C. E.; Kroon, J. *J. Mol. Struct.* **1997**, *395*, 289–295.
262. Ott, K.-H.; Meyer, B. *J. Comput. Chem.* **1996**, *17*, 1068–1084.
263. Spieser, S. A. H.; van Kuik, J. A.; Kroon-Batenburg, L. M. J.; Kroon, J. *Carbohydr. Res.* **1999**, *322*, 264–273.
264. Howard, E. I.; Grigera, J. R. *Carbohydr. Res.* **1996**, *282*, 25–40.
265. Lins, R. D.; Hünenberger, P. H. *J. Comput. Chem.* **2005**, *26*, 1400–1412.
266. Pereira, C. S.; Kony, D.; Baron, R.; Müller, M.; van Gunsteren, W. F.; Hünenberger, P. H. *Biophys. J.* **2006**, *90*, 4337–4344.
267. Molinero, V.; Goddard, W. A., III. *J. Phys. Chem. B* **2004**, *108*, 1414–1427.
268. Molinero, V.; Goddard, W. A., III. *ACS Symp. Ser.* **2006**, *930*, 271–284.
269. Molteni, C.; Parrinello, M. *J. Am. Chem. Soc.* **1998**, *120*, 2168–2171.
270. lonescu, A. R.; Bérces, A.; Zgierski, M. Z.; Whitfield, D. M.; Nukada, T. *J. Phys. Chem. A* **2005**, *109*, 8096–8105.
271. MacKerell, D. A. *J. Comput. Chem.* **2004**, *25*, 1584–1604.
272. Tschampel, S. M.; Kirschner, K. N.; Woods, R. J. *ASC Symp. Ser.* **2006**, *930*, 235–257.
273. Pérez, S.; Imberty, A.; Engelsen, S. B.; Gruza, J.; Mazeau, K.; Jimenez-Barbero, J.; Poveda, A.; Espinosa, J.-F.; van Eyck, B. P.; Johnson, G.; French, A. D.; Kouwijzer, M. L. C. E.; Grootenuis, P. D. J.; Bernardi, A.; Raimondi, L.; Senderowitz, H.; Durier, V.; Vergoten, G.; Rasmussen, K. *Carbohydr. Chem.* **1998**, *314*, 141–155.
274. Hemmingsen, L.; Madsen, D. E.; Esbensen, A. L.; Olsen, L.; Engelsen, S. B. *Carbohydr. Res.* **2004**, *339*, 937–948.
275. Kouwijzer, M. L. C. E.; van Eijck, B. P.; Kroon, J. *J. Comput. Chem.* **1993**, *14*, 1281–1289.
276. van Eijck, B. P.; Kroon, E. J. *J. Comput. Chem.* **1999**, *20*, 799–812.
277. Behler, J.; Price, D. W.; Drew, M. G. B. *Phys. Chem. Chem. Phys.* **2001**, *3*, 588–601.
278. Corzana, F.; Motawia, M. S.; Hervé du Penhoat, C.; Perez, S.; Tschampel, S. M.; Woods, R. J.; Engelsen, S. B. *J. Comput. Chem.* **2004**, *25*, 573–586.
279. Brady, J. W. *J. Am. Chem. Soc.* **1986**, *108*, 8153–8160.
280. Ha, S. N.; Madsen, L. J.; Brady, J. W. *Biopolymers* **1988**, *27*, 1927–1952.
281. Schmidt, R. K.; Teo, B.; Brady, J. W. *J. Phys. Chem.* **1995**, *99*, 11339–11343.
282. Hardy, B. J.; Gutierrez, A.; Lesiak, K.; Seidl, E.; Wildmalm, G. *J. Phys. Chem.* **1996**, *100*, 9187–9192.
283. van Eijck, B. P.; Mooij, W. T. M.; Kroon, J. *Acta Crystallogr., Sect. B* **1995**, *51*, 99–103.
284. Caffarena, E. G.; Grigera, J. R. *Carbohydr. Res.* **1997**, *300*, 51–57.
285. Roberts, C. J.; Debenedetti, P. G. *J. Phys. Chem. B* **1999**, *103*, 7308–7318.
286. Höchtl, P.; Boresch, S.; Steinhauser, O. *J. Chem. Phys.* **2000**, *112*, 9810–9821.
287. Weingärtner, H.; Knocks, A.; Boresch, S.; Höchtl, P.; Steinhauser, O. *J. Chem. Phys.* **2001**, *115*, 1463–1472.
288. Ekdawi-Sewer, N. C.; Conrad, P. B.; De Pablo, J. J. *J. Phys. Chem. A* **2001**, *105*, 734–742.
289. Molinero, V.; Çağin, T.; Goddard, W. A., III. *Chem. Phys. Lett.* **2003**, *377*, 469–474.
290. Molinero, V.; Çağin, T.; Goddard, W. A., III. *J. Phys. Chem. A* **2004**, *108*, 3699–3712.
291. Lerbret, A.; Bordat, P.; Affouard, F.; Descamps, M.; Migliardo, F. *J. Phys. Chem. B* **2005**, *109*, 11046–11057.
292. Molinero, V.; Goddard, W. A., III. *Phys. Rev. Lett.* **2005**, *95*, 045701/1–045701/4.
293. Brady, J. W. *J. Am. Chem. Soc.* **1989**, *111*, 5155–5165.
294. Kroon-Batenburg, L. M. J.; Kroon, J. *Biopolymers* **1990**, *29*, 1243–1248.
295. Ha, S.; Gao, J.; Tidor, B.; Brady, J. W.; Karplus, M. *J. Am. Chem. Soc.* **1991**, *113*, 1553–1557.
296. Schmidt, R. K.; Karplus, M.; Brady, J. W. *J. Am. Chem. Soc.* **1996**, *118*, 541–546.
297. Liu, Q.; Schmidt, R. K.; Karplus, P. A.; Brady, J. W. *J. Am. Chem. Soc.* **1997**, *119*, 7851–7862.
298. Sidhu, K. S.; Goodfellow, J. M.; Turner, J. Z. *J. Chem. Phys.* **1999**, *110*, 7943–7950.
299. Astley, T.; Birch, G. G.; Drew, M. G. B.; Rodger, P. M. *J. Phys. Chem. A* **1999**, *103*, 5080–5090.
300. Naidoo, K. J.; Kuttel, M. *J. Comput. Chem.* **2001**, *4*, 445–456.
301. Best, R. B.; Jackson, G. E.; Naidoo, K. J. *J. Phys. Chem. B* **2001**, *105*, 4742–4751.
302. Cheetham, N. W. H.; Dasgupta, P.; Ball, G. E. *Carbohydr. Res.* **2003**, *338*, 955–962.
303. Yu, H.; Amann, M.; Hansson, T.; Köhler, J.; Wich, G.; van Gunsteren, W. F. *Carbohydr. Res.* **2004**, *339*, 1697–1709.

304. Christen, M.; Kunz, A.-P. E.; van Gunsteren, W. F. *J. Phys. Chem. B* **2006**, *110*, 8488–8498.
305. Gonzalez-Outeirino, J.; Kirschner, K. N.; Thobhani, S.; Woods, R. J. *Can. J. Chem.* **2006**, *84*, 569–579.
306. Choi, Y.; Cho, K. W.; Jeong, K.; Jung, S. *Carbohydr. Res.* **2006**, *341*, 1020–1028.
307. Scares, T. A.; Hünenberger, P. H.; Kastenholz, M. A.; Kräutler, V.; Lenz, T.; Lins, R. D.; Oostenbrink, C.; van Gunsteren, W. F. *J. Comput. Chem.* **2005**, *26*, 725–737.
308. Schüler, L. D.; Daura, X.; van Gunsteren, W. F. *J. Comput. Chem.* **2001**, *22*, 1205–1218.
309. Chandrasekhar, I.; Kastenholz, M. A.; Lins, R. D.; Oostenbrink, C.; Schüler, L. D.; Tieleman, D. P.; van Gunsteren, W. F. *Eur. Biophys. J.* **2003**, *32*, 67–77.
310. Ryckaert, J.-P.; Ciccotti, G.; Berendsen, H. J. C. *J. Comput. Phys.* **1977**, *23*, 327–341.
311. Yun-yu, S.; Lu, W.; van Gunsteren, W. F. *Mol. Simulat.* **1988**, *1*, 369–383.
312. Berendsen, H. J. C.; Postma, J. P. M.; van Gunsteren, W. F.; Hermans, J. Interaction models for water in relation to protein hydration. In *Intermolecular Forces*; Pullman, B., Ed.; Reidel: Dordrecht, The Netherlands, 1981; pp 331–342.
313. Barker, J. A.; Watts, R. O. *Mol. Phys.* **1973**, *26*, 789–792.
314. Tironi, I. G.; Sperb, R.; Smith, P. E.; van Gunsteren, W. F. *J. Chem. Phys.* **1995**, *102*, 5451–5459.
315. Glättli, A.; Daura, X.; van Gunsteren, W. F. *J. Chem. Phys.* **2002**, *116*, 9811–9828.
316. Heinz, T. N.; van Gunsteren, W. F.; Hiinenberger, P. H. *J. Chem. Phys.* **2001**, *115*, 1125–1136.
317. Berendsen, H. J. C.; Postma, J. P. M.; van Gunsteren, W. F.; DiNola, A.; Haak, J. R. *J. Chem. Phys.* **1984**, *81*, 3684–3690.
318. Kirkwood, J. G. *J. Chem. Phys.* **1935**, *3*, 300–313.
319. King, P. M. Free energy via molecular simulation: a primer. In *Computer Simulation of Biomolecular Systems, Theoretical and Experimental Applications*; van Gunsteren, W. F., Weiner, P. K., Wilkinson, A. J., Eds.; ESCOM Science, B.V.: Leiden, The Netherlands, 1993; Vol. 2, pp 267–314.
320. van Gunsteren, W. F.; Beutler, T. C.; Fraternali, F.; King, P. M.; Mark, A. E.; Smith, P. E. Computation of free energy in practice: choice of approximations and accuracy limiting factors. In *Computer Simulation of Biomolecular Systems, Theoretical and Experimental Applications*; van Gunsteren, W. F., Weiner, P. K., Wilkinson, A. J., Eds.; Vol. 2; ESCOM Science, B.V.: Leiden, The Netherlands, 1993; pp 315–367.
321. Allen, M. P.; Tildesley, D. J. *Computer Simulation of Liquids*; Oxford University Press: New York, 1987.
322. Kearsley, S. A. *Acta Crystallogr., Sect. A* **1989**, *45*, 208–210.
323. W.L. DeLano. The PYMOL molecular visualization system. http://www.pymol.org/.
324. V. Kräutler, M.A. Kastenholz, and P.H. Hünenberger. The ESRA molecular mechanics analysis package, 2005. http://esra.sf.net/.
325. Yamada, H.; Tanigakiuchi, K.; Nagao, K.; Okajima, K.; Mukae, T. *Tetrahedron Lett.* **2004**, *45*, 9207–9209.
326. Bhacca, N. S.; Horton, D.; Paulsen, H. *J. Org. Chem.* **1968**, *33*, 2484–2487.
327. Holland, C. V.; Horton, D.; Jewell, J. S. *J. Am. Chem. Soc.* **1967**, *32*, 1818–1821.
328. Perlin, A. S.; Casu, B.; Sanderson, G. R.; Tse, J. *Carbohydr. Res.* **1972**, *21*, 123–132.
329. Anibarro, M.; Gessler, K.; Uson, I.; Sheldrick, G. M.; Harata, K.; Uekama, K.; Hirayama, F.; Abe, Y.; Saenger, W. *J. Am. Chem. Soc.* **2001**, *123*, 11854–11862.
330. Lamba, D.; Segre, A. L.; Ragazzi, M.; Ferro, D. R.; Toffanin, R. *Carbohydr. Res. C* **1991**, *209*, 13–15.
331. Zhang, Q.; Narszalek, E. *J. Am. Chem. Soc.* **2006**, *128*, 5596–5597.
332. Polavarapu, P. L.; Ewig, C. S. *J. Comput. Chem.* **1985**, *13*, 1255–1261.
333. Cramer, C. J.; Truhlar, D. G. *J. Am. Chem. Soc.* **1993**, *115*, 5745–5753.
334. Jebber, K. A.; Zhang, K.; Cassady, C. J.; Chung-Phillips, A. *J. Am. Chem. Soc.* **1996**, *118*, 10515–10524.
335. Barrows, S. E.; Storer, J. W.; Cramer, C. J.; French, A. D.; Truhlar, D. G. *J. Comput. Chem.* **1998**, *19*, 1111–1129.
336. Wladowski, B. D.; Chenoweth, S. A.; Jones, K. E.; Brown, J. W. *J. Phys. Chem. A* **1998**, *102*, 5086–5092.
337. Lii, J.-H.; Ma, B.; Allinger, N. L. *J. Comput. Chem.* **1999**, *20*, 1593–1603.
338. Talbot, F. O.; Simons, J. P. *Phys. Chem. Chem. Phys.* **2002**, *4*, 3562–3565.
339. Corchado, J. C.; Sánchez, M. L.; Aguilar, M. A. *J. Am. Chem. Soc.* **2004**, *126*, 7311–7319.
340. Macleod, N. A.; Johannessen, C.; Hecht, L.; Barren, L. D.; Simons, J. P. *Int. J. Mass Spectrom.* **2006**, *253*, 193–200.
341. Csonka, G. I.; Kolossváry, L.; Császár, P.; Éliás, K.; Csizmadia, I. G. *J. Mol. Struct.* **1997**, *395*, 29–40.
342. Appell, M.; Willett, J. L. *Carbohydr. Res.* **2005**, *340*, 459–468.
343. Rahal-Sekkal, M.; Sekkal, N.; Kleb, B. C.; Bleckmann, P. *J. Comput. Chem.* **2003**, *24*, 806–818.
344. Jockusch, R. A.; Talbot, F. O.; Simons, J. P. *Phys. Chem. Chem. Phys.* **2003**, *5*, 1502–1507.
345. Momany, F. A.; Appell, M.; Willett, J. L.; Schnupf, U.; Bosnia, W. B. *Carbohydr. Res.* **2006**, *341*, 525–537.
346. Sturdy, Y. K.; Skylaris, C.-K.; Clary, D. C. *J. Phys. Chem. B* **2006**, *110*, 3485–3492.
347. Ohanessian, J.; Avenel, D.; Kanters, J. A.; Smits, D. *Acta Crystallogr., Sect. B* **1977**, *33*, 1063–1066.
348. Jockusch, R. A.; Kroemer, R. T.; Talbot, F. O.; Simons, J. P. *J. Phys. Chem. A* **2003**, *107*, 10725–10732.
349. Matsuo, K.; Gekko, K. *Carbohydr. Res.* **2004**, *339*, 591–597.
350. Mrcheussault, R. H.; Pérez, S. *Biopolymers* **1979**, *18*, 2369–2374.
351. Rockwell, G. D. *J. Am. Chem. Soc.* **1998**, *120*, 100953–100963.
352. Tvaroška, I.; Carver, J. P. *J. Phys. Chem. B* **1997**, *101*, 2992–2999.
353. Tvaroška, I.; Kožar, T. *Theor. Chim. Acta* **1986**, *70*, 99–114.
354. Streefkerk, D. G.; Stephen, A. M. *Carbohydr. Res.* **1976**, *49*, 13–25.
355. Bock, K.; Fernandez, J.; Guzman, B. *Carbohydr. Res.* **1986**, *174*, 354–359.
356. Morales, E. Q.; Padrón, J. I.; Trujillo, M.; Vásquez, J. T. *J. Org. Chem.* **1995**, *60*, 2537–2548.
357. Padron, J.; Vazquez, J. T. *Chirality* **1997**, *9*, 626–637.
358. Zuccarello, F.; Buemi, G. *Carbohydr. Res.* **1995**, *273*, 129–145.
359. Danilova, V. A.; Istomina, N. V.; Krivdin, L. B. *Russ. J. Org. Chem.* **2004**, *40*, 1194–1199.
360. Ejchart, A.; Dabrowski, J. *Magn. Reson. Chem.* **1992**, *30*, S115–S124.
361. Momany, F. A.; Appell, M.; Strati, G.; Willett, J. L. *Carbohydr. Res.* **2004**, *339*, 553–567.

362. Samuel, J.; Tanner, M. E. *Nat. Prod. Rep.* **2001**, *19*, 261–277.
363. Tewari, Y. B.; Goldberg, R. N. *Biophys. Chem.* **1986**, *24*, 291–294.
364. Angyal, S. J. *Carbohydr. Res.* **1997**, *300*, 279–281.
365. Petrus, L.; Petrusova, M.; Hricoviniova, Z. *Top. Curr. Chem.* **2001**, *215*, 15–41.
366. Osanai, S. *Top. Curr. Chem.* **2001**, *215*, 43–76.
367. Hricoviniova, Z. *Carbohydr. Res.* **2006**, *341*, 2131–2134.
368. Bilik, V. *Chem. Zvesti* **1972**, *26*, 183.
369. Bilik, V.; Voelter, W.; Bayer, E. *Liebigs Ann. Chem.* **1974**, *1974*, 1162–1166.
370. Barone, G.; Cacace, P.; Castronuovo, G.; Elia, V. *Carbohydr. Res.* **1981**, *91*, 101–111.
371. Miyajima, K.; Sawada, M.; Nakagaki, M. *Bull. Chem. Soc. Jpn.* **1983**, *56*, 1620–1623.
372. Janado, M.; Yano, Y. *J. Solution Chem.* **1985**, *14*, 891–902.
373. van Doren, H. A.; Galema, S. A.; Engberts, B. F. N. *Langmuir* **1995**, *11*, 687–688.